

Entangled states from quantum algebra $\mathcal{U}_h(\mathfrak{sl}(2, \mathbb{R}))$

A. BALLESTEROS¹, J.J. RELANCIO^{2,3} AND L. SANTAMARÍA-SANZ²

¹Departamento de Física, Universidad de Burgos, 09001 Burgos, Spain

²Departamento de Matemáticas y Computación, Universidad de Burgos, 09001 Burgos, Spain

³Centro de Astropartículas y Física de Altas Energías (CAPA), Universidad de Zaragoza, Zaragoza 50009, Spain

e-mail: angelb@ubu.es, jjrelancio@ubu.es, lssanz@ubu.es

Abstract

We discuss the application of the Jordanian quantum algebra $\mathcal{U}_h(\mathfrak{sl}(2, \mathbb{R}))$, as a Hopf algebra deformation of the Lie algebra $\mathfrak{sl}(2, \mathbb{R})$, in the context of entanglement properties of quantum states. For them, several kind of entanglement measures and fidelities are obtained, parametrized by the deformation parameter h . In particular, we construct the associated h -deformed Dicke states on $\mathfrak{sl}(2, \mathbb{R})$, comparing them to the q -Dicke states obtained from the quantum deformation of the $\mathcal{U}_q(\mathfrak{sl}(2, \mathbb{R}))$. Moreover, the density matrices of these h -deformed Dicke states are compared to the experimental realizations of those of Dicke states. A similar behavior is observed, pointing out that the h -deformation could be used to describe noise and decoherence effects in experimental settings.

1 Introduction

Quantum algebras are deformations of Hopf algebras [1], and they can also be regarded as the Hopf algebra duals of quantum groups, which generalize classical Lie groups into the non-commutative domain [2, 3]. These quantum algebras are constructed by deforming not only the commutation relations but also the coproduct (which governs how tensor product representations are formed) of the universal enveloping algebra of a given Lie algebra. This deformation is controlled by a so-called quantum parameter [4, 5]. Originally introduced as new symmetry structures in (1+1)-dimensional quantum integrable field theories, these algebras have since found a wide range of applications in exactly solvable spin chains, nuclear physics, non-commutative geometry, and quantum gravity [6–11]. The interpretation of the deformation parameter varies depending on the specific physical context.

A cornerstone in the study of quantum algebras is the quantum deformation of the Lie algebra $\mathfrak{sl}(2, \mathbb{R})$, which serves as the prototype of this theory. There are two fundamentally different types of deformations. The first is the standard or quasitriangular deformation, denoted $\mathcal{U}_q(\mathfrak{sl}(2, \mathbb{R}))$, which was the earliest to be introduced [12] and has received the most attention, particularly in relation to its applications. The second is the non-standard deformation, often referred to as the triangular or Jordanian deformation, represented as $\mathcal{U}_h(\mathfrak{sl}(2, \mathbb{R}))$, and this version will be the focus of the present work. Each of these deformations corresponds to a distinct constant solution of the Classical Yang-Baxter Equation on $\mathfrak{sl}(2, \mathbb{R})$ [2]. It is important to emphasize that the irreducible representations of the standard quantum algebra $\mathcal{U}_q(\mathfrak{sl}(2, \mathbb{R}))$ share a structural resemblance with those of the undeformed Lie algebra $\mathfrak{sl}(2, \mathbb{R})$, provided that the deformation parameter q is not a root of unity [13]. However, this similarity does not extend to the non-standard quantum algebra $\mathcal{U}_h(\mathfrak{sl}(2, \mathbb{R}))$ or its associated quantum group [14–17]. The finite-dimensional irreducible representations of $\mathcal{U}_h(\mathfrak{sl}(2, \mathbb{R}))$ have been investigated in [18–21], and results concerning their tensor product decompositions and Clebsch–Gordan coefficients are available in [21, 22]. In addition, infinite-dimensional representations have been analyzed in [20, 21]. One of the distinctive features of the $\mathcal{U}_q(\mathfrak{sl}(2, \mathbb{R}))$ deformation is its non-Hermitian character, which naturally raises questions about its relation to \mathcal{PT} -symmetry. For finite-dimensional cases, this issue has been recently addressed in [23], where \mathcal{PT} -symmetric Hamiltonians were constructed for general finite-dimensional irreducible representations of the non-standard \mathcal{U}_h quantum algebra, leading to a new class of exactly solvable models with real spectra. Its generalization to infinite-dimensional representations is studied in [24].

Observables of a system in quantum theories are often organized into an algebra as a set of operators with specific commutation relations. The study of entanglement measures in the context of quantum theories is a very active field of research within theoretical physics since the 30s, specially in the context of one-dimensional many body quantum systems [25–28]. Entanglement basically describes the non-classical correlations between different parts of a system. In the algebraic approach, observables of these parts or subsystems are subalgebras of the full algebra of observables. States that are invariant under transformations generated by a symmetry algebra often have special entanglement properties. When the symmetry is deformed, the algebraic relations and, consequently, the set of invariant states are altered. This can lead to new classes of entangled states and may require modified entanglement criteria or witnesses that respect the deformed symmetry. There exists many measures of entanglement (entanglement entropy, Rényi entropy, concurrence, fidelity, purity, negativity...), each of one is suitable for different situations depending on the nature of the quantum state (i.e. mixed or pure), the value of certain parameters (i.e. finite or zero temperature) and the nature of the partition (complementary or non-complementary regions). In this work, we will focus on the simplest setup. Let $|\Psi\rangle$ be a pure state of a 1+1D QFT and let us define a bipartition of space into two complementary regions A and \bar{A} so that the Hilbert space of the theory \mathcal{H} also decomposes into a direct product $\mathcal{H}_A \otimes \mathcal{H}_{\bar{A}}$. Then the reduced density matrix associated to subsystem A is obtained by tracing out the degrees of freedom of subsystem \bar{A} as

$$\rho_A = \text{Tr}_{\bar{A}}(|\Psi\rangle\langle\Psi|), \quad (1)$$

and the von Neumann (or entanglement) and n th Rényi entropy of a subsystem A are defined as

$$S = -\text{Tr}_A(\rho_A \log \rho_A) \quad \text{and} \quad S_n = \frac{\log(\text{Tr}_A \rho_A^n)}{1-n}. \quad (2)$$

Moreover, the fidelity F between two states with density matrices ρ, σ is symmetric under the exchange of both of them, and can be obtained from

$$F(\rho, \sigma) = \left(\text{tr} \sqrt{\sqrt{\rho} \sigma \sqrt{\rho}} \right)^2. \quad (3)$$

For pure states, as the ones we will use in this work, the previous equation reduces to

$$F(\rho, \sigma) = |\langle \psi_\rho | \psi_\sigma \rangle|^2, \quad (4)$$

where $|\psi_\rho\rangle$ and $|\psi_\sigma\rangle$ are the states that generate ρ and σ , respectively. So the fidelity between pure states gives the probability of finding the state $|\psi_\rho\rangle$ when measuring $|\psi_\sigma\rangle$ in a basis containing $|\psi_\rho\rangle$. Among the most studied quantum states, a special interest has been put in Dicke states, which are the fully symmetric eigenstates of the total spin operators in $SU(2)$ theories. Dicke states $|D_N^k\rangle$ are those that are invariant under the permutation group. For a system of N qubits with k excitations, the corresponding Dicke state in the undeformed theory reads

$$|D_N^k\rangle := \sqrt{\frac{k!(N-k)!}{N!}} \sum_l \mathcal{P}_l \left(|\downarrow\rangle^{\otimes(N-k)} \otimes |\uparrow\rangle^{\otimes k} \right), \quad (5)$$

where $\sum_l \mathcal{P}_l$ denotes sum under the relevant permutation group. Due to their symmetry, Dicke states are exceptionally valuable in quantum computing because they combine (i) strong multipartite entanglement with (ii) robustness against particle loss and (iii) metrological enhancement [29–32]. In this work, we will study these measures of entanglement in order to compare the results in some undeformed and deformed Dicke states.

This paper is organized as follows. Sec. 2 discusses the mathematical structure of the undeformed and deformed $\mathcal{U}_q(\mathfrak{sl}(2, \mathbb{R}))$ and $\mathcal{U}_h(\mathfrak{sl}(2, \mathbb{R}))$ algebras, including their commutation relations, coproducts, and representations. It also covers the construction of Dicke states in both undeformed and deformed settings from the Clebsch–Gordan coefficients for the deformed case. Sec. 3 examines the explicit construction of two-qubit states under the h -deformation, analyzes their properties

(such as orthogonality and symmetry), and compares them with undeformed and q -deformed cases. This section also includes a discussion on Schmidt decomposition for these states. Sec. 4 extends the analysis to three-qubit systems, presenting the explicit forms of the h -deformed states, their symmetries, and classification according to the Acin scheme for multipartite entanglement. In Sec. 5 we give an analytical expression for computing the h -Dicke states for up to eleven spins and for a infinite spin systems. Furthermore, in Sec. 6 we analyze the von Neumann entropy, Rényi entropies, and fidelity for undeformed, q -deformed, and h -deformed Dicke states to discuss how deformation affects entanglement. Finally, we end with some conclusions and further work in Sec. 7.

2 Revisiting $\mathcal{U}(\mathfrak{sl}(2, \mathbb{R}))$, $\mathcal{U}_q(\mathfrak{sl}(2, \mathbb{R}))$ and $\mathcal{U}_h(\mathfrak{sl}(2, \mathbb{R}))$ Hopf algebras

The special unitary group of degree n , denoted $SU(n)$, is the Lie group of $n \times n$ unitary matrices with determinant 1. The Lie algebra structure $\mathfrak{sl}(2, \mathbb{R})$ is defined by the following commutation relations

$$[J_z, J_{\pm}] = \pm J_{\pm}, \quad [J_+, J_-] = 2J_z, \quad (6)$$

where

$$J_x = \frac{1}{2}\sigma_x, \quad J_y = \frac{1}{2}\sigma_y, \quad J_z = \frac{1}{2}\sigma_z, \quad J_{\pm} = J_x \pm iJ_y, \quad (7)$$

is the usual 2×2 dimensional irreducible representation in term of the Pauli matrices [33, 34]

$$\sigma_x = \begin{pmatrix} 0 & 1 \\ 1 & 0 \end{pmatrix}, \quad \sigma_y = \begin{pmatrix} 0 & -i \\ i & 0 \end{pmatrix}, \quad \sigma_z = \begin{pmatrix} 1 & 0 \\ 0 & -1 \end{pmatrix}. \quad (8)$$

The action of the spin operators J on the basis vectors of the finite dimensional Hilbert space¹ \mathbb{C}^2

$$\left\{ |\uparrow\rangle := \begin{pmatrix} 1 \\ 0 \end{pmatrix}, \quad |\downarrow\rangle := \begin{pmatrix} 0 \\ 1 \end{pmatrix} \right\} \quad (9)$$

is given by

$$\begin{aligned} J_+ |\downarrow\rangle &= |\uparrow\rangle, & J_+ |\uparrow\rangle &= |\downarrow\rangle, \\ J_- |\downarrow\rangle &= |\downarrow\rangle, & J_- |\uparrow\rangle &= |\downarrow\rangle, \\ J_z |\downarrow\rangle &= -\frac{1}{2} |\downarrow\rangle, & J_z |\uparrow\rangle &= \frac{1}{2} |\uparrow\rangle. \end{aligned} \quad (10)$$

The Hopf algebra structure of $\mathcal{U}(\mathfrak{sl}(2, \mathbb{R}))$ is given by the commutation relations (6) together with the coproduct map $\Delta_0 : \mathcal{U}(\mathfrak{sl}(2, \mathbb{R})) \rightarrow \mathcal{U}(\mathfrak{sl}(2, \mathbb{R})) \otimes \mathcal{U}(\mathfrak{sl}(2, \mathbb{R}))$ defined as

$$\Delta_0(J_{\pm}) = 1 \otimes J_{\pm} + J_{\pm} \otimes 1, \quad \Delta_0(J_z) = 1 \otimes J_z + J_z \otimes 1, \quad (11)$$

a counit $\epsilon : \mathcal{U}(\mathfrak{sl}(2, \mathbb{R})) \rightarrow \mathbb{C}$, and an antihomomorphism called antipode $\gamma : \mathcal{U}(\mathfrak{sl}(2, \mathbb{R})) \rightarrow \mathcal{U}(\mathfrak{sl}(2, \mathbb{R}))$ such that:

$$\epsilon(J_z) = \epsilon(J_{\pm}) = 0, \quad \epsilon(1) = 1, \quad \gamma(J_z) = -J_z, \quad \gamma(J_{\pm}) = -J_{\pm}, \quad \gamma(1) = 1. \quad (12)$$

Notice that the coproduct is coassociative, *i.e.* $(\Delta \otimes \text{id})\Delta = (\text{id} \otimes \Delta)\Delta$ (see more properties in [35]). Multiparticle states in $\mathfrak{sl}(2, \mathbb{R})$ can be obtained in the usual way [36] through the spin- j irreducible representation of $\mathfrak{sl}(2, \mathbb{R})$ as

$$|j, m\rangle = C_{m_1, m_2, m}^{j_1, j_2, j} |j_1, m_1\rangle \otimes |j_2, m_2\rangle, \quad (13)$$

where $j_i = 0, 1/2, 1, 3/2, \dots$, $m_i = -j_i, \dots, j_i$, and $C_{m_1, m_2, m}^{j_1, j_2, j}$ are the associated Clebsch–Gordan coefficients

$$\begin{aligned} C_{m_1, m_2, m}^{j_1, j_2, j} &= \delta_{m_1 + m_2, m} \left(\frac{(j_1 + j_2 - j)!(j_1 - j_2 + j)!(-j_1 + j_2 + j)!}{(j_1 + j_2 + j + 1)!} \right)^{1/2} \\ &\times ((j_1 + m_1)!(j_1 - m_1)!(j_2 + m_2)!(j_2 - m_2)!(j + m)!(j - m)!(2j + 1))^{1/2} \\ &\times \sum_k \frac{(-1)^k}{k!(j_1 + j_2 - j - k)!(j_1 - m_1 - k)!(j_2 + m_2 - k)!(j - j_2 + m_1 + k)!(j - j_1 - m_2 + k)!}. \end{aligned} \quad (14)$$

¹A set of N spins is quantum mechanically described by rays in the finite dimensional Hilbert space \mathbb{C}^{2^N} .

Concerning deformations, the Hopf algebra $\mathcal{U}_q(\mathfrak{sl}(2, \mathbb{R}))$ is generated by $\{L_z, L_+, L_-\}$, and can be defined in terms of the following relations [35] where $q \in \mathbb{R}^+$:

$$[L_z, L_{\pm}] = \pm L_{\pm}, \quad [L_+, L_-] = [2L_z]_q = \frac{q^{L_z} - q^{-L_z}}{q^{1/2} - q^{-1/2}}. \quad (15)$$

Above, we have made use of the q -number

$$[n]_q := \frac{q^{n/2} - q^{-n/2}}{q^{1/2} - q^{-1/2}}, \quad (16)$$

so

$$[2L_z]_q = \frac{q^{L_z} - q^{-L_z}}{q^{1/2} - q^{-1/2}} = 2L_z + o[q^2], \quad (17)$$

and we recover the $\mathfrak{sl}(2, \mathbb{R})$ Lie algebra in the $q \rightarrow 1$ limit. The coalgebra structure for the $\mathcal{U}_q(\mathfrak{sl}(2, \mathbb{R}))$ algebra is generated by the deformed coproduct map

$$\Delta(L_{\pm}) = q^{-L_z/2} \otimes L_{\pm} + L_{\pm} \otimes q^{L_z/2}, \quad \Delta(L_z) = 1 \otimes L_z + L_z \otimes 1. \quad (18)$$

The counit is the same as in the undeformed case. Regarding the antipode, we can see that:

$$\gamma(L_z) = -L_z, \quad \gamma(L_{\pm}) = -q^{\mp 1/2} L_{\pm}, \quad \gamma(1) = 1. \quad (19)$$

Irreducible representations for $\mathcal{U}_q(\mathfrak{sl}(2, \mathbb{R}))$ are defined through the action of the algebra generators onto an state $|j, m\rangle$ in the form

$$L_{\pm}|j, m_i\rangle := \sqrt{[j_i \mp m_i]_q [j_i \pm m_i + 1]_q} |j, m_i \pm 1\rangle, \quad L_z|j, m_i\rangle = m_i|j, m_i\rangle. \quad (20)$$

For states of the form (13), the q -Clebsch–Gordan coefficients (see [37] and references therein) are to be used:

$$\begin{aligned} \mathcal{C}_{m_1, m_2, m}^{j_1, j_2, j}(q) &= \delta_{m, m_1 + m_2} q^{\frac{1}{2}(j_1 m_2 - j_2 m_1) - \frac{1}{4}(-j + j_1 + j_2)(j + j_1 + j_2 + 1)} \\ &\sqrt{\frac{[2j + 1]_q [j + m]_q! [j_2 - m_2]_q! [j + j_1 - j_2]_q! [-j + j_1 + j_2]_q! [j + j_1 + j_2 + 1]_q!}{[j - m]_q! [j_1 - m_1]_q! [j_1 + m_1]_q! [j_2 + m_2]_q! [j - j_1 + j_2]_q!}} \\ &\sum_{n=0}^{\min(-j + j_1 + j_2, j_2 - m_2)} \frac{[2j_2 - n]_q! (-1)^{-j + j_1 + j_2 + n} q^{\frac{1}{2}n(j_1 + m_1)} [j_1 + j_2 - m - n]_q!}{[n]_q! [j_2 - m_2 - n]_q! [-j + j_1 + j_2 - n]_q! [j + j_1 + j_2 - n + 1]_q!}. \end{aligned} \quad (21)$$

Moreover, the deformed Casimir operator for the algebra (15) reads

$$C_q = L_- L_+ + [L_z]_q [L_z + 1]_q = L_+ L_- + [L_z]_q [L_z - 1]_q, \quad (22)$$

and the eigenvalues of C_q in the representation states $|j, m\rangle$ are just $[j]_q [j + 1]_q$. Therefore, if q is not a root of unity, the representation theory of $\mathfrak{sl}(2, \mathbb{R})_q(2)$ is just structurally the same as that of $\mathfrak{sl}(2, \mathbb{R})$ (see [35]). Regarding the construction of Dicke states in this deformation, we will denote the tensor product state of N qubits with k excitations (\uparrow) as $|n_1, \dots, n_k\rangle$ where n_i denotes the positions of each one of the k excitations within the N -th tensor product. Thus $n_i \in \{1, \dots, N\}$ while $i \in \{1, \dots, k\}$. In this way, the q -Dicke states can be written as [38]:

$$|D_N^k\rangle_q = \sqrt{\frac{[k]_q! [N - k]_q!}{[N]_q!}} \sum_{\mathbf{n}} q^{-k(\frac{N+1}{4}) + \frac{1}{2} \sum_{i=1}^k n_i} |\mathbf{n}\rangle, \quad (23)$$

where the sum runs over all the possible sets $\mathbf{n} = (n_1, \dots, n_k)$ describing the location of the k excitations. In the following sections, we will compute the Dicke states in the non-standard deformation $\mathcal{U}_h(\mathfrak{sl}(2, \mathbb{R}))$ in order to compare both deformations.

On the other hand, the Hopf algebra $\mathcal{U}_h(\mathfrak{sl}(2, \mathbb{R}))$ is generated by $\{X, Y, H\}$, and can be defined in terms of the following relations [16]

$$[H, X] = \frac{2}{h} \sinh(hX), \quad [H, Y] = -Y \cosh(hX) - \cosh(hX)Y, \quad [X, Y] = H, \quad (24)$$

being $h \in \mathbb{R}$ the deformation parameter. The coproducts are given by:

$$\begin{aligned} \Delta(X) &= X \otimes 1 + 1 \otimes X, \\ \Delta(Y) &= Y \otimes e^{hX} + e^{-hX} \otimes Y, \\ \Delta(H) &= H \otimes e^{hX} + e^{-hX} \otimes H. \end{aligned} \quad (25)$$

Under the change of basis

$$Z_+ = \frac{2}{h} \tanh\left(\frac{hX}{2}\right), \quad Z_- = \cosh\left(\frac{hX}{2}\right) Y \cosh\left(\frac{hX}{2}\right), \quad (26)$$

the above commutators transforms into the usual ones for $\mathfrak{sl}(2, \mathbb{R})$, as displayed in Eq. (6), providing $H = 2J_z$, $Z_\pm = J_\pm$. The generators $\{H, Z_\pm\}$ act on the basis (9) exactly the same as the generators of $\mathcal{U}(\mathfrak{sl}(2, \mathbb{R}))$, i.e. by means of (10). Therefore, the entire effect of the deformation is encoded by the action on multipartite states.

The $\mathcal{U}_h(\mathfrak{sl}(2, \mathbb{R}))$ co-algebra structure is given by the coproduct map, which reads [39]

$$\begin{aligned} \Delta(H) &= H \otimes 1 + 1 \otimes H + 2H \otimes \sum_{n=1}^{\infty} \left(\frac{hZ_+}{2}\right)^n + \sum_{n=1}^{\infty} \left(-\frac{hZ_+}{2}\right)^n \otimes 2H, \\ \Delta(Z_+) &= (1 \otimes Z_+ + Z_+ \otimes 1) \left(\sum_{n=0}^{\infty} \left(-\frac{h^2}{4}\right)^n Z_+^n \otimes Z_+^n \right), \\ \Delta(Z_-) &= Z_- \otimes \sum_{n=0}^{\infty} (n+1) \left(\frac{hZ_+}{2}\right)^n + \sum_{n=0}^{\infty} (n+1) \left(-\frac{hZ_+}{2}\right)^n \otimes Z_- \\ &\quad + h \left(C - \frac{H^2}{4}\right) \otimes \sum_{m=1}^{\infty} m \left(\frac{hZ_+}{2}\right)^m - \sum_{m=1}^{\infty} m \left(-\frac{hZ_+}{2}\right)^m \otimes h \left(C - \frac{H^2}{4}\right) \\ &\quad + \left(\frac{h}{2}\right)^2 Z_+ Z_- Z_+ \otimes \sum_{k=2}^{\infty} (k-1) \left(\frac{hZ_+}{2}\right)^k + \sum_{k=2}^{\infty} (k-1) \left(-\frac{hZ_+}{2}\right)^k \otimes \left(\frac{h}{2}\right)^2 Z_+ Z_- Z_+, \end{aligned} \quad (27)$$

where $C = Z_+ Z_- + H^2/4 - H/2$ is the Casimir element. In the limit $h \rightarrow 0$ we recover the primitive coproduct (11). For all the previous coproducts, if we denote $\Delta^{(2)} \equiv \Delta$, then the homomorphism $\Delta^{(3)} : A \rightarrow A \otimes A \otimes A$ can be defined through any of the two following equivalent expressions:

$$\Delta^{(3)} := (1 \otimes \Delta^{(2)}) \circ \Delta^{(2)} = (\Delta^{(2)} \otimes 1) \circ \Delta^{(2)}. \quad (28)$$

This can be generalized to any number N of tensor products of A either by the next recurrence relation

$$\Delta^{(N)} := (1^{\otimes(N-2)} \otimes \Delta^{(2)}) \circ \Delta^{(N-1)}, \quad (29)$$

or, equivalently, by

$$\Delta^{(N)} := (\Delta^{(2)} \otimes 1^{\otimes(N-2)}) \circ \Delta^{(N-1)}. \quad (30)$$

The Clebsch–Gordan coefficients for $\mathcal{U}_h(\mathfrak{sl}(2, \mathbb{R}))$ (denoted by $\mathcal{C}_{n_1, n_2, m}^{j_1, j_2, j}(h)$) can be derived from those of $\mathcal{U}(\mathfrak{sl}(2, \mathbb{R}))$ by means of [40]

$$\mathcal{C}_{n_1, n_2, m}^{j_1, j_2, j}(h) = \sum_{m_1 + m_2 = m} \mathcal{C}_{m_1, m_2, m}^{j_1, j_2, j} A_{n_1 - m_1, n_2 - m_2}^{m_1, m_2}, \quad (31)$$

where

$$\begin{aligned}
A_{k,l}^{m_1,m_2} &= a_{k,l}^{m_1,m_2} \frac{\alpha_{j_1,m_1+k} \alpha_{j_2,m_2+l}}{\alpha_{j_1,m_1} \alpha_{j_2,m_2}}, \\
\alpha_{j,m} &= \sqrt{\frac{(j+m)!}{(j-m)!}}, \\
a_{k,l}^{m_1,m_2} &= (-1)^k 2^{-k-l} h^{k+l} (b_{k,l}^{m_1,m_2} - b_{k-1,l-1}^{m_1,m_2}), \\
b_{k,l}^{m_1,m_2} &= \begin{cases} \frac{(-2m_1-k)_l (-2m_2-l)_k}{k!l!} & \text{if } k \geq 0 \text{ and } l \geq 0, \\ 0 & \text{otherwise.} \end{cases}
\end{aligned} \tag{32}$$

Note that the h -Clebsch–Gordan coefficients give in general non-normalized states.

3 2-qubit h -states

Consider the space resulting from the tensor product of two ($N = 2$) spaces of spin=1/2. Applying $\Delta(Z_-)$ to the state of highest weight ($\uparrow\uparrow$) one could systematically obtain all the new states $|D_{N=2}^H\rangle$, where the superindex refers to the eigenvalue of the H operator associated to this state. Another way to compute these states is by using the Clebsch–Gordan coefficients of the undeformed theory and equations (31), (32). We find the following normalized states:

$$\begin{aligned}
|D_2^{-2}\rangle_h &= \frac{4}{h^2+4} \left(\frac{h^2}{4} |\uparrow\uparrow\rangle - \frac{h}{2} |\uparrow\downarrow\rangle + \frac{h}{2} |\downarrow\uparrow\rangle + |\downarrow\downarrow\rangle \right), \\
|D_2^0\rangle_h &= \frac{1}{\sqrt{2}} (|\uparrow\downarrow\rangle + |\downarrow\uparrow\rangle), \\
|D_2^2\rangle_h &= |\uparrow\uparrow\rangle, \\
|M_2^0\rangle_h &= \frac{1}{\sqrt{h^2+2}} (-h |\uparrow\uparrow\rangle + |\uparrow\downarrow\rangle - |\downarrow\uparrow\rangle).
\end{aligned} \tag{33}$$

We have used the notation shown in Fig. 1 for label the states.

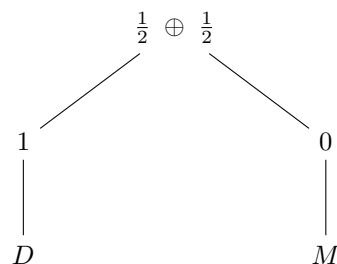


Figure 1: Coupling tree for two spin- $\frac{1}{2}$ particles, showing $J = 1, 0$ states, labeled as D and M , respectively.

Notice that the singlet (M) and triplet (D) subspaces are not orthogonal to each other, contrary to what happens in the undeformed theory. However, the same structure that the one presented in [20] for a mixed representation of the deformation appears. This basically consists on states that are undeformed $\{|D_2^0\rangle_h, |D_2^2\rangle_h\}$ mixed with the rest of states, in which there is a combination of deformed components and original components of the undeformed state. We will call h -Dicke states those obtained from the irreducible representation with highest dimension. Notice that due to the relative minus sign in the terms proportional to h , $|D_2^{-2}\rangle_h$ is no longer a full-symmetric state, as does not happen in the undeformed case. Furthermore, there is a crucial difference with respect

to the standard deformation theory, in which the normalized states $|D_{N=2}^{Lz}\rangle_q$ of the singlet and the triplet read [41]

$$\begin{aligned}
|D_2^{-1}\rangle_q &= |\downarrow\downarrow\rangle, \\
|D_2^0\rangle_q &= \frac{1}{\sqrt{[2]_q}}(q^{1/4}|\downarrow\uparrow\rangle + q^{-1/4}|\uparrow\downarrow\rangle), \\
|D_2^1\rangle_q &= |\uparrow\uparrow\rangle, \\
|M_2^0\rangle_q &= \frac{1}{\sqrt{[2]_q}}(-q^{-1/4}|\downarrow\uparrow\rangle + q^{1/4}|\uparrow\downarrow\rangle).
\end{aligned} \tag{34}$$

Considering the above q -deformed states, there are one most probable state within the usual basis given by $\{|\uparrow\uparrow\rangle, |\uparrow\downarrow\rangle, |\downarrow\uparrow\rangle, |\downarrow\downarrow\rangle\}$, and the others are exponentially less probable (due to the explicit form of q -numbers (16)). But for the non-standard deformation theory we do not see such monotonicity in the probability of obtaining each of the four possible states of the basis of two spins. In fact, all the coefficients of the lineal combination of basic vectors in $|D_N^H\rangle$ in (33) are different. Remember that in $\mathfrak{sl}(2, \mathbb{R})$ the J_z operator represents the z component of the spin operator and their eigenvalues are the quantum number m , i.e. $J_z|jm\rangle = m|jm\rangle$. Notice that now, all the states in (33) are eigenvectors of the deformed J_z , i.e., $(J_z)_h |D_N^H\rangle = \Delta(H) |D_N^H\rangle = m_h |D_N^H\rangle$. We can observe that the states $\{|D_2^0\rangle_h, |D_2^2\rangle_h\}$ (characterised by $j = 1$) are the usual Dicke ones. Furthermore, $|D_2^{-2}\rangle_h$ (being $j = 1$) is symmetric under the exchange $h \rightarrow -h$ when $|ik\rangle \rightarrow |ki\rangle$. We will call it h -Dicke state. On the other hand, the state on the singlet $|M_2^0\rangle_h$ remains unchanged when $|ik\rangle \rightarrow |ki\rangle$ if we also make $h \rightarrow -h$ and add a global sign.

Figure 2 shows the density matrix of the pure undeformed Bell state $|\Psi^-\rangle = (|\uparrow\downarrow\rangle - |\downarrow\uparrow\rangle)/\sqrt{2}$ as well as the corresponding q - and h -deformed states $|M_2^0\rangle$ for $q = h = 0.5$. As usual, the diagonal squares (i.e. ρ_{ii}) represent the populations or occupancy probabilities of each base state. The off-diagonal elements (ρ_{ij} , with $i \neq j$) represent the quantum coherences or interference amplitudes between the states. Interestingly, this kind of diagrams are experimentally achievable (see

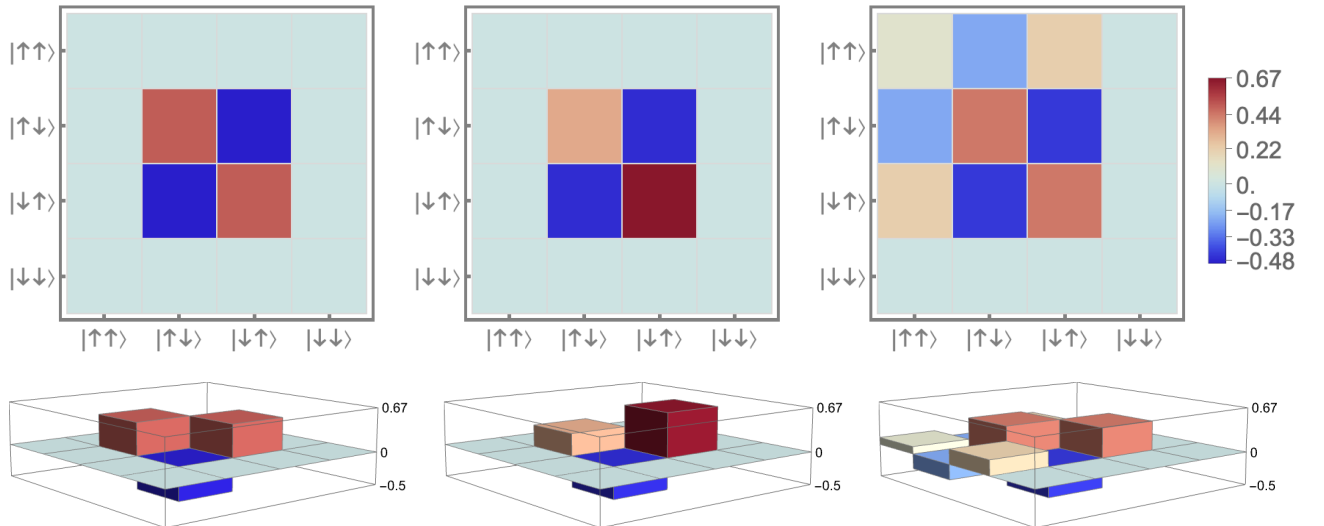


Figure 2: Left: Undeformed Bell state $|\Psi^-\rangle = (|\uparrow\downarrow\rangle - |\downarrow\uparrow\rangle)/\sqrt{2}$. Middle: Corresponding q -deformed state $|M_2^0\rangle_q$ for $q = 0.5$. Right: Corresponding h -deformed state $|M_2^0\rangle_h$ for $h = 0.5$.

for instance Fig. 3 in [42]). The experimental setup involves two spatially separated atomic ensembles, synchronized laser pulses for entanglement generation, photon interference at a beam splitter, heralded entanglement creation, and quantum state tomography [43] to verify the entangled state. Fig. 3 in [42] presents the density matrix associated with the entangled state stored between two

distant atomic ensembles, as inferred from experimental data. This matrix is quite close to our q -Dicke state $|M_2^0\rangle_{q=0.5}$. Moreover, [44] reports the first experimental demonstration of universal quantum logic operations between electron spins bound to individual phosphorus donors in silicon. Donor atoms' electron spins serve as the qubits whose quantum states and gate operations are characterized in Fig. 5. of [44]. The system is controlled and read out using standard semiconductor techniques, including electron spin resonance (ESR) for qubit manipulation and a single-electron transistor (SET) for high-fidelity, single-shot spin readout. The histograms concerning the measured probabilities of the spin states of the two-electron qubit system being found in each computational basis state after a two-qubit gate operation in Fig. 5 of that work are more reminiscent of the non-symmetric configurations obtained with the h -deformed states $|M_2^0\rangle_h$ which we propose here. The results in [44] pave the way for larger-scale silicon-based quantum computers using donor electron spins. In both papers, the entanglement criteria can be studied in terms of density matrix elements. In addition, in [45] the Dicke state $|D_4^2\rangle$ is studied using, as a source of the four photons, the second order emission of collinear type II spontaneous parametric down conversion (SPDC) [46]. This is done by applying an ultraviolet laser to pump a barium-borate crystal. In another vein, quantum error correction codes have been used in quantum state tomography [47, 48]. Indeed, based on permutationally invariant tomography [49], the Dicke states of six spins are experimentally obtained using SPDC techniques. Moreover, in [50], the introduction of a threshold in quantum tomography reduces the number of measurements required for constructing a density matrix with a good accuracy (around 99%).

In quantum computing applications, Dicke states have been prepared using IBM quantum computers in [51, 52]. In those papers, similar density matrices of those obtained in this work appear. Therefore, the states we propose in this section and our characterization of them allow us to visualize this density matrix directly and to compare with the experimental thresholds of the papers. We hope to explore this possibility in future works.

3.1 The Schmidt decomposition classification

Here we present in detail the identification of our states with the Schmidt decomposition [53–55]. The Schmidt decomposition provides a way to represent any pure state of a bipartite quantum system as a sum of product states that are mutually orthogonal, constructed from suitable local bases for each subsystem. This approach ensures that the expansion uses only the minimal set of necessary product states, with no redundancy. In order to make it clear, we start with a two-qubit state $|\varphi_\theta\rangle$ in the undeformed scenario, which reads

$$|\varphi_\theta\rangle = \cos\theta |\uparrow\uparrow\rangle + \sin\theta |\downarrow\downarrow\rangle = \begin{pmatrix} \cos\theta \\ 0 \\ 0 \\ \sin\theta \end{pmatrix}, \quad \theta \in \left[0, \frac{\pi}{4}\right]. \quad (35)$$

In this context, $|ii\rangle$ denotes the product state $|i\rangle_A \otimes |i\rangle_B$, where both sets of local basis states, $\{|i\rangle\}_A$ and $\{|i\rangle\}_B$, are chosen specifically for the given two-qubit state $|\varphi_\theta\rangle$. Any relative phase can be incorporated into either local basis. By convention, the state $|\uparrow\uparrow\rangle$ is associated with the largest (or equal largest) Schmidt coefficient. A greater value of the parameter θ corresponds to a higher degree of entanglement. Altogether, a pure two-qubit state is characterized by six real parameters: the entanglement parameter θ , a hidden relative phase, and two parameters for each local basis, once normalization and the global phase have been fixed.

The Schmidt decomposition is rather important. In large-scale simulations—such as those employing matrix product states, the density matrix renormalization group, or general tensor network techniques—maintaining the Schmidt decomposition at each system bipartition enables one to optimally truncate the less relevant degrees of freedom [56]. This approach ensures computational efficiency by retaining only the most significant contributions to the entanglement spectrum. Furthermore, the Schmidt form is invaluable for designing optimal local operations. For any protocol

that manipulates the quantum state—such as teleportation, entanglement concentration, or conversions between local and classical resources—knowledge of the Schmidt decomposition directly identifies which local unitaries to implement and with what probabilities, thereby enabling precise control over the transformation process [57].

For the non-trivial h -deformed state of the triplet in (33), we define two local unitary operators U_1 (acting on the first qubit) and U_2 (acting on the second qubit), whose explicit matrix forms are

$$U_1 = \begin{pmatrix} \frac{4}{b} & -\frac{4+h^2+a}{hb} \\ \frac{4+h^2+a}{hb} & -\frac{4}{b} \end{pmatrix}, \quad U_2 = \begin{pmatrix} \frac{a-4+h^2}{hc} & \frac{4}{c} \\ -\frac{4}{c} & \frac{a-4+h^2}{hc} \end{pmatrix}, \quad (36)$$

where

$$a = \sqrt{16 + 24h^2 + h^4}, \quad b = \sqrt{16 + \frac{(4 + h^2 + a)^2}{h^2}}, \quad c = \sqrt{16 + \frac{(4 + h^2 - a)^2}{h^2}}. \quad (37)$$

These unitaries are chosen so that

$$|\tilde{D}_2^{-2}\rangle_h = U_1 \otimes U_2 |D_2^{-2}\rangle_h, \quad (38)$$

transforms the original state into its canonical Schmidt form

$$|\tilde{D}_2^{-2}\rangle_h = \begin{pmatrix} \frac{-a^2+(h^2-4)a}{8a} \\ 0 \\ 0 \\ \frac{-a^2-(h^2-4)a}{8a} \end{pmatrix}. \quad (39)$$

Here the state has been written as a column vector with only two non-zero components, which are precisely the Schmidt coefficients.

Similarly, for the h -deformed state of the singlet in (33) we find

$$|\tilde{M}_2^0\rangle_h = U_1 \otimes U_2 |M_2^0\rangle_h, \quad (40)$$

where

$$U_1 = \begin{pmatrix} \frac{\sqrt{2}}{d} & \frac{-h+\sqrt{4+h^2}}{\sqrt{2d}} \\ \frac{h-\sqrt{4+h^2}}{\sqrt{2d}} & \frac{\sqrt{2}}{d} \end{pmatrix}, \quad U_2 = \begin{pmatrix} \frac{-h+\sqrt{4+h^2}}{\sqrt{2d}} & \sqrt{2}d \\ -\frac{h+\sqrt{4+h^2}}{\sqrt{2d}} & -\frac{h+\sqrt{4+h^2}}{\sqrt{2d}} \end{pmatrix}, \quad (41)$$

and

$$d = \sqrt{4 + h^2 - h\sqrt{4 + h^2}}. \quad (42)$$

Again, we can write the state into its Schmidt decomposition form as

$$|\tilde{M}_2^0\rangle_h = \begin{pmatrix} \frac{\sqrt{2}}{d} \\ 0 \\ 0 \\ \frac{1}{\sqrt{2}} \end{pmatrix}. \quad (43)$$

Up to individual phase factors on each $|i\rangle_A$ and $|i\rangle_B$ the Schmidt decomposition is unique. This simplifies the comparison of states and the classification of families of states based on their coefficients. For the deformed states analyzed in this section, the Schmidt decomposition yields exactly two nonzero Schmidt coefficients. Since the Schmidt rank is greater than 1 we know that both deformed states remain entangled (i.e., they are not separable).

4 3-qubit h -states

Consider the space resulting from the tensor product of three spaces of spin=1/2. We obtain the following states:

$$\begin{aligned}
|D_3^{-3}\rangle_h &= \frac{4}{\sqrt{19h^4 + 32h^2 + 16}} \left(\frac{3h^2}{4} |\uparrow\uparrow\downarrow\rangle - \frac{h^2}{4} |\uparrow\downarrow\uparrow\rangle - h |\uparrow\downarrow\downarrow\rangle + \frac{3h^2}{4} |\downarrow\uparrow\uparrow\rangle + h |\downarrow\downarrow\uparrow\rangle + |\downarrow\downarrow\downarrow\rangle \right), \\
|D_3^{-1}\rangle_h &= \frac{4\sqrt{3}}{\sqrt{9h^4 + 32h^2 + 48}} \left(\frac{\sqrt{3}h^2}{4} |\uparrow\uparrow\uparrow\rangle - \frac{h}{\sqrt{3}} |\uparrow\uparrow\downarrow\rangle + \frac{h}{\sqrt{3}} |\downarrow\uparrow\uparrow\rangle + \frac{1}{\sqrt{3}} (|\uparrow\downarrow\downarrow\rangle + |\downarrow\uparrow\downarrow\rangle + |\downarrow\downarrow\uparrow\rangle) \right), \\
|D_3^1\rangle_h &= \frac{1}{\sqrt{3}} (|\uparrow\uparrow\downarrow\rangle + |\uparrow\downarrow\uparrow\rangle + |\downarrow\uparrow\uparrow\rangle), \\
|D_3^3\rangle_h &= |\uparrow\uparrow\uparrow\rangle, \\
|M_3^{-1}\rangle_h &= \frac{\sqrt{6}}{\sqrt{5h^2 + 6}} \left(\frac{1}{\sqrt{6}} (-h |\uparrow\uparrow\downarrow\rangle - 2h |\downarrow\uparrow\uparrow\rangle) + \frac{1}{\sqrt{6}} (|\uparrow\downarrow\downarrow\rangle + |\downarrow\uparrow\downarrow\rangle - 2 |\downarrow\downarrow\uparrow\rangle) \right), \\
|M_3^1\rangle_h &= \frac{\sqrt{2}}{\sqrt{3h^2 + 2}} \left(-\frac{3h}{\sqrt{6}} |\uparrow\uparrow\uparrow\rangle + \frac{1}{\sqrt{6}} (2 |\uparrow\uparrow\downarrow\rangle - |\uparrow\downarrow\uparrow\rangle - |\downarrow\uparrow\uparrow\rangle) \right), \\
|V_3^{-1}\rangle_h &= \frac{\sqrt{2}}{\sqrt{h^2 + 2}} \left(-\frac{h}{\sqrt{2}} |\uparrow\uparrow\downarrow\rangle + \frac{1}{\sqrt{2}} (|\downarrow\uparrow\downarrow\rangle - |\uparrow\downarrow\downarrow\rangle) \right), \\
|V_3^1\rangle_h &= \frac{\sqrt{2}}{\sqrt{h^2 + 2}} \left(-\frac{h}{\sqrt{2}} |\uparrow\uparrow\uparrow\rangle + \frac{1}{\sqrt{2}} (|\downarrow\uparrow\uparrow\rangle - |\uparrow\downarrow\uparrow\rangle) \right). \tag{44}
\end{aligned}$$

We have used the notation shown in Fig. 3 for label the states. The only Dicke states are again

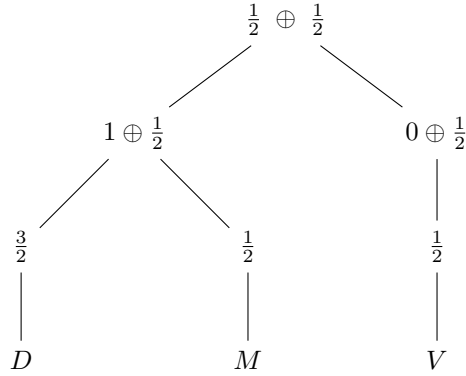


Figure 3: Coupling tree for three spin- $\frac{1}{2}$ particles, with final labels D , M and V .

the undeformed ones $\{|D_3^1\rangle_h, |D_3^3\rangle_h\}$. The states $\{|D_3^{-3}\rangle_h, |D_3^{-1}\rangle_h\}$ ($j = 3/2$) are symmetric under the exchange $h \rightarrow -h$ when $|ilk\rangle \rightarrow |kli\rangle$. They will be also called h -Dicke states. Furthermore, we again observe that the states $\{|V_3^{-1}\rangle_h, |V_3^1\rangle_h\}$ ($j = 1/2$) remain unchanged when $|ilk\rangle \rightarrow |lik\rangle$ if we also make $h \rightarrow -h$ and add a global sign. This last symmetry does not hold for the other two states: $|M_3^1\rangle_h$ is invariant under the change $|ilk\rangle \rightarrow |lik\rangle$ and $|M_3^{-1}\rangle_h$ has not a clear symmetry.

Notice that as the value of h increases the state moves further and further away from its undeformed analogue (see Fig. 4). The experimental results of [51] resemble our state $\{|D_3^{-1}\rangle_h$ for small h .

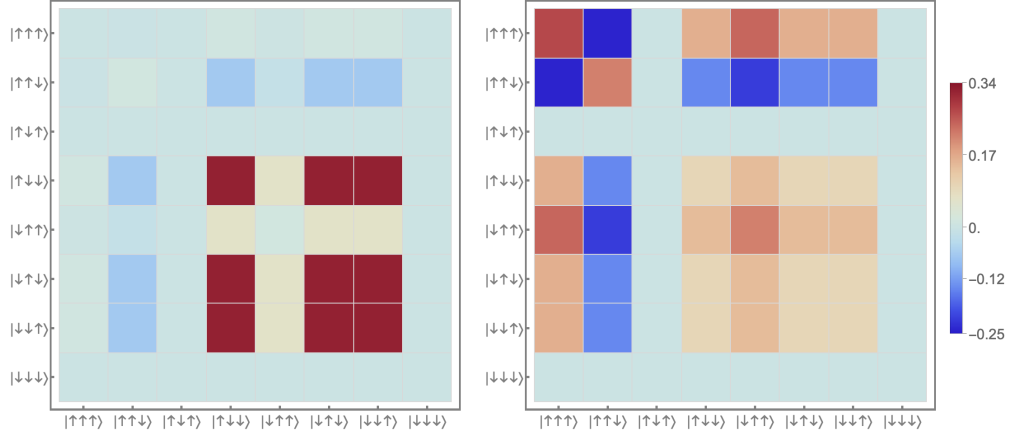


Figure 4: Density matrix for $\{|D_3^{-1}\rangle_h$ for $h = 0.2$ (left) and $h = 1.5$.

4.1 Acín classification

It is possible to generalize the Schmidt decomposition to three qubits [55]. The result is called Acín decomposition. In this way, any tripartite spin system can be reduced to the form

$$|\phi\rangle_{\lambda_i, \varphi} = \lambda_0 |\uparrow\uparrow\uparrow\rangle + \lambda_1 e^{i\varphi_1} |\downarrow\uparrow\uparrow\rangle + \lambda_2 |\downarrow\uparrow\downarrow\rangle + \lambda_3 |\downarrow\downarrow\uparrow\rangle + \lambda_4 |\downarrow\downarrow\downarrow\rangle, \quad (45)$$

where $\lambda_i \geq 0$, $0 \leq \varphi \leq \pi$, $\sum_{i=0}^4 \lambda_i^2 = 1$.

Our objective in this section is defining three local unitary operators U_1 (acting on the first qubit), U_2 (acting on the second qubit), and U_3 (acting on the third qubit) so that $U_1 \otimes U_2 \otimes U_3$ transforms the original h -deformed state into its canonical Acín form (45). The information is collected in Tables 1 and 2 in Appendix A.

5 Description of the general states

The calculation of the Clebsch–Gordan coefficients for larger numbers of qubits could be done in an analogous way following the bootstrap program explained in the first section of this article (Eqs. (13), (14), (31), (32)). For instance, Table 3 in Appendix B shows the configuration of states of 4 qubits as a linear combination of the elements of the basic basis (in the first row of the table) with the associated Clebsch–Gordan coefficients. Note the following notation for states:

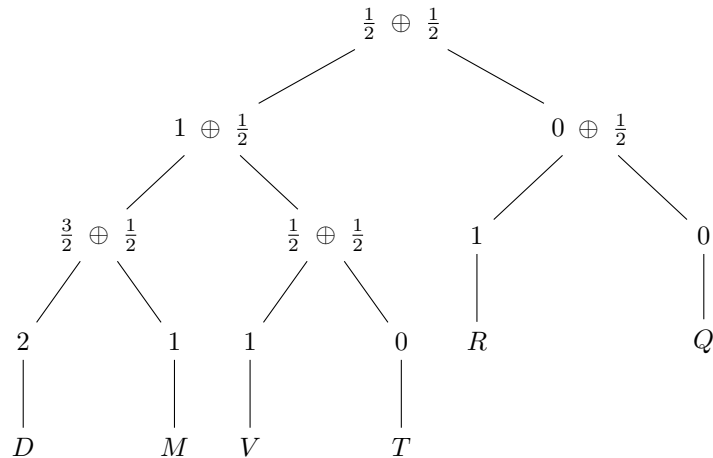


Figure 5: Four spin-1/2 coupling tree with vertical lines to end state labels.

Although one could obtain all the Clebsch–Gordan coefficients for an arbitrary state of N qubits through the bootstrap program, there is another way to obtain the h -Dicke states that arise from

composing N 1/2-spins. Generally, when composing spins in quantum mechanics, one calculates the state with highest value of J_z and maximum eigenvalue of J and from there one applies the downward staircase operator to obtain all the others. But for the h -deformed states notice that the coproduct of Z_- is much more complicated than the one concerning Z_+ in (27). Furthermore, for angular momentum equal to 1/2 the coproduct of Z_+ is simply $\Delta(Z_+) = 1 \otimes Z_+ + Z_+ \otimes 1$ because $Z_+ |\uparrow\rangle = 0$. Hence, if we calculate the lowest state of the highest eigenvalue of H , we can find all the h -Dicke deformed states (always labeled in this work as $|D\rangle_h$ states²) from it by simply applying the coproduct $\Delta(Z_+)$. We will describe all the steps in detail below.

We consider now a system of N qubits. The quantum state of interest (lowest state of the multiplet $|D\rangle_h$ of maximum eigenvalue of the H operator) is a superposition of computational basis states $|S\rangle = |s_1 s_2 \dots s_N\rangle$ (where $s_k \in \{\uparrow, \downarrow\}$ for $1 \leq k \leq N$):

$$|D_N^{-N}\rangle_h = \sum_S \chi^{-N}(S) |S\rangle. \quad (46)$$

The coefficients $\chi^{-N}(S)$ have a particular structure related to the number of \uparrow states (n_\uparrow) in the state $|S\rangle$. Let $P_\uparrow(S) = \{k | s_k = \uparrow\}$ be the set of indices where state S has an ' \uparrow ', and $n_\uparrow(S) = |P_\uparrow(S)|$ (the cardinal of the set). The structure of the coefficient is:

$$\chi^{-N}(S) = \gamma(S) \left(\frac{h}{2}\right)^{n_\uparrow(S)}, \quad (47)$$

where $\gamma(S)$ is a factor (generally integer) that depends on N and the specific configuration of \uparrow and \downarrow states in S (i.e., on the set $P_\uparrow(S)$).

5.1 General Formula for $\gamma(S)$

We have discovered that $\gamma(S)$ can be elegantly expressed using elementary symmetric polynomials. We define the function $f(k)$ for an index k :

$$f(k) = 2k - N - 1. \quad (48)$$

For a state $|S\rangle$ with n_\uparrow states at positions $P_\uparrow(S)$, we define $e_m(P_\uparrow(S))$ as the m -th elementary symmetric polynomial of the values $\{f(k) | k \in P_\uparrow(S)\}$:

$$\begin{aligned} e_0(P_\uparrow) &= 1, \\ e_1(P_\uparrow) &= \sum_{k_1 \in P_\uparrow} f(k_1), \\ e_2(P_\uparrow) &= \sum_{k_1 < k_2 \in P_\uparrow} f(k_1) f(k_2), \\ &\dots \\ e_m(P_\uparrow) &= \sum_{k_1 < k_2 < \dots < k_m \in P_\uparrow} f(k_1) f(k_2) \dots f(k_m). \end{aligned} \quad (49)$$

By convention, $e_m(P_\uparrow) = 0$ if $m > n_\uparrow$.

The factor $\gamma(S)$ for a state with n_\uparrow \uparrow states at positions P_\uparrow is given by the sum:

$$\gamma_{n_\uparrow}(P_\uparrow) = \sum_{m=0}^{\lfloor n_\uparrow/2 \rfloor} C_m(N) e_{n_\uparrow-2m}(P_\uparrow), \quad (50)$$

²For instance, if $N = 3$ the state $|\Psi_N\rangle$ will correspond to $|D_3^{-3}\rangle_h$ in (44). Notice that the procedure we explain in this section is only valid for states $|D\rangle_h$, i.e. the ones with maximum value of H for a given composition of N spins. We are only interested in these states here because when $h \rightarrow 0$ we will recover the usual Dicke states in the undeformed scenario. This is not the case for the $|M\rangle_h, |V\rangle_h$ states in the $N = 3$ case (and analogously the reasoning is applied for the other multiplets for other values of $N \neq 3$).

where $C_m(N)$ are polynomial coefficients in N .

We have determined the first six coefficients $C_m(N)$ by analyzing the data for $N = 2$ up to $N = 11$:

$$\begin{aligned}
C_0(N) &= 1, \\
C_1(N) &= N, \\
C_2(N) &= N(3N - 2), \\
C_3(N) &= N(15N^2 - 30N + 16), \\
C_4(N) &= N(105N^3 - 420N^2 + 588N - 272), \\
C_5(N) &= N(945N^4 - 6300N^3 + 16380N^2 - 18960N + 7936).
\end{aligned} \tag{51}$$

The leading term of $C_m(N)$ is $(2m - 1)!!N^m$, where $(2m - 1)!!$ is the odd double factorial.

5.2 Explicit formulas for n_\uparrow up to 11

Using the general formula (50) and the known coefficients $C_m(N)$ we can compute γ_{n_\uparrow} :

- $\gamma_0 = C_0e_0 = 1,$
- $\gamma_1 = C_0e_1 = e_1,$
- $\gamma_2 = C_0e_2 + C_1e_0 = e_2 + N,$
- $\gamma_3 = C_0e_3 + C_1e_1 = e_3 + Ne_1,$
- $\gamma_4 = C_0e_4 + C_1e_2 + C_2e_0 = e_4 + Ne_2 + N(3N - 2),$
- $\gamma_5 = C_0e_5 + C_1e_3 + C_2e_1 = e_5 + Ne_3 + N(3N - 2)e_1,$
- $\gamma_6 = C_0e_6 + C_1e_4 + C_2e_2 + C_3e_0 = e_6 + Ne_4 + N(3N - 2)e_2 + N(15N^2 - 30N + 16),$
- $\gamma_7 = C_0e_7 + C_1e_5 + C_2e_3 + C_3e_1 = e_7 + Ne_5 + N(3N - 2)e_3 + N(15N^2 - 30N + 16)e_1,$
- $\gamma_8 = C_0e_8 + C_1e_6 + C_2e_4 + C_3e_2 + C_4e_0 = e_8 + Ne_6 + N(3N - 2)e_4 + N(15N^2 - 30N + 16)e_2 + N(105N^3 - 420N^2 + 588N - 272),$
- $\gamma_9 = C_0e_9 + C_1e_7 + C_2e_5 + C_3e_3 + C_4e_1 = e_9 + Ne_7 + N(3N - 2)e_5 + N(15N^2 - 30N + 16)e_3 + N(105N^3 - 420N^2 + 588N - 272)e_1,$
- $\gamma_{10} = C_0e_{10} + C_1e_8 + C_2e_6 + C_3e_4 + C_4e_2 + C_5e_0 = e_{10} + Ne_8 + N(3N - 2)e_6 + N(15N^2 - 30N + 16)e_4 + N(105N^3 - 420N^2 + 588N - 272)e_2 + N(945N^4 - 6300N^3 + 16380N^2 - 18960N + 7936),$
- $\gamma_{11} = C_0e_{11} + C_1e_9 + C_2e_7 + C_3e_5 + C_4e_3 + C_5e_1 = e_{11} + Ne_9 + N(3N - 2)e_7 + N(15N^2 - 30N + 16)e_5 + N(105N^3 - 420N^2 + 588N - 272)e_3 + N(945N^4 - 6300N^3 + 16380N^2 - 18960N + 7936)e_1.$

5.3 Dicke states for n_\uparrow up to 11

All the Dicke states can be obtained from the repeated application of the $\Delta^{(N)}(Z_+)$. From Eq. (27), and taking into account that

$$Z_+^2 |\downarrow\rangle = 0 \tag{52}$$

for 1/2 spins, the coproduct for N particles can be written in a very simple form

$$\begin{aligned}
\Delta^{(N)}(Z_+) &= \sum_{i=1}^N \left(1^{\otimes(i-1)} \otimes Z_+ \otimes 1^{\otimes(N-i)} \right) \\
&\quad - \frac{\hbar^2}{2} \sum_{1 \leq i < j < k \leq N} \left(1^{\otimes(i-1)} \otimes Z_+ \otimes 1^{\otimes(j-i-1)} \otimes Z_+ \otimes 1^{\otimes(k-j-1)} \otimes Z_+ \otimes 1^{\otimes(N-k)} \right).
\end{aligned}$$

Then, one can construct the others h -Dicke states by repeatedly applying this coproduct to $|D_N^{-N}\rangle_h$. Any h -Dicke state $|D_N^{-N+i+1}\rangle_h$ can be obtained from $|D_N^{-N+i}\rangle_h$ just by summing all its possible flips on one spin (\downarrow to \uparrow) plus all its possible flips on three spins multiplied by $-h^2/2$. After normalization of the states, one can check that for all the cases shown here ($N = 2, 3, 4$) this formula is valid.

5.4 Considerations for large N

For a fixed number of \uparrow states n_\uparrow and a very large N , there are some caveats that are worth stressing:

- As the position k at which there is a qubit \uparrow increases, and if it does so proportionally to N (i.e. xN), then the polynomial $f(k) \approx N(2x - 1)$, the elementary symmetric polynomials $e_m(P_\uparrow)$ scales as N^m , and $C_m(N)$ scales as $(2m - 1)!!N^m$. Consequently, in the summation $\gamma_{n_\uparrow} = \sum_{m=0}^{\lfloor n_\uparrow/2 \rfloor} C_m(N)e_{n_\uparrow-2m}$, the m -th term scales as $N^m \times N^{n_\uparrow-2m} = N^{n_\uparrow-m}$.
- The dominant term for $N \rightarrow \infty$ is the $m = 0$ term, i.e. the highest power term of N , which is e_{n_\uparrow} . This is nothing but the product of $f(k)$ for all the positions where there is an \uparrow qubit. Therefore, in this asymptotic limit: $\gamma_{n_\uparrow}(P_\uparrow) \approx e_{n_\uparrow}(P_\uparrow) = \prod_{k \in P_\uparrow} (2k - N - 1)$. The terms with $m \geq 1$ are corrections that become less relevant as N grows much larger than n .

In conclusion, when N is very large, one can ignore the correction terms and quickly calculate the leading coefficients of the deformed Dicke states. This is especially useful in quantum systems with many qubits, where the corrections are negligible and the principal behavior is dominated by the simplest term.

6 Entropy and fidelity

The aim of this section is to study some measures of entanglement between the h -deformed states presented in Secs. 3 and 4. The methodology will always start by obtaining the density matrix of the state by means of $|\Psi\rangle\langle\Psi|$. Then, for the states of two qubits we will assume a bipartition of the whole system in such a way that each qubit corresponds to a different subsystem. Later, we will compute the reduced density matrix associated to subsystem A (the first qubit in the tensor product) by tracing out the degrees of freedom of the complementary subsystem (i.e. the second qubit) and diagonalize the resulting matrix. This is so because for diagonal matrices, the formulae of von Neumann and Rényi entropies are much simpler:

$$S = - \sum_i \lambda_i \log \lambda_i, \quad S_n = \frac{1}{1-n} \log \left(\sum_i \lambda_i^n \right), \quad (53)$$

being λ_i the eigenvalues of the reduced density matrix. On the other hand, the fidelity between states will be computed from the entire (not reduced) density matrices associated to the given states by means of Eq. (3).

For instance, the von Neumann and Rényi entropies for $|M_2^0\rangle_h$ and $|D_2^{-2}\rangle_h$ can be written as:

$$\begin{aligned} S_n(|M_2^0\rangle_h) &= \frac{1}{1-n} [\log(\Lambda_+^n + \Lambda_-^n)], & S(|M_2^0\rangle_h) &= -\Lambda_+ \log \Lambda_+ - \Lambda_- \log \Lambda_-, \\ S_n(|D_2^{-2}\rangle_h) &= \frac{1}{1-n} [\log(\Omega_+^n + \Omega_-^n)], & S(|D_2^{-2}\rangle_h) &= -\Omega_+ \log \Omega_+ - \Omega_- \log \Omega_-, \\ \Lambda_\pm &= \frac{h^2 \pm \sqrt{h^2 + 4h} + 2}{2h^2 + 4}, & \Omega_\pm &= \frac{h^4 + 8h^2 \pm (h^2 - 4)\sqrt{h^4 + 24h^2 + 16} + 16}{2(h^2 + 4)^2}. \end{aligned} \quad (54)$$

Note that all of the above formulas are even functions in h . The Rényi and von Neumann entropies of the h -deformed states for two qubits are shown in Fig. 6 as a function of the deformation parameter. It is important to remember that for $h \rightarrow 0$ the undeformed Dicke states are obtained. Consequently, $|M_2^0\rangle_h$ transforms into the Bell state $(|\uparrow\downarrow\rangle - |\downarrow\uparrow\rangle)/\sqrt{2}$, for which the entanglement

entropy is maximum [58], viz $\log 2$ (as can be seen in the vertical axis of Fig. 6 and in the blue line of Fig. 7). On the other hand, $|D_2^{-2}\rangle_h$ transforms into $|\downarrow\downarrow\rangle$, with associated zero entanglement entropy. Moreover, for $|M_2^0\rangle_h$ Rényi entropies decrease monotonically as h increases. Contrary, for $|D_2^{-2}\rangle_h$ entropy increases, reaches a maximum at $|h| = 2$, and then decreases towards zero with increasing h . In both cases, in the limit $h \rightarrow \infty$ entropy tends to zero, which implies that the state becomes product (without entanglement). This shows that the deformation h can control the degree of entanglement of quantum states. The different colour curves (blue, red, green, brown, yellow) show how the Rényi entropy changes when varying the index n . The higher the n , the curves tend to slightly smaller values, but retain the general shape. The von Neumann entropy (dashed black line) is always above the Rényi entropies with $n > 1$, which is consistent with their mathematical definitions.

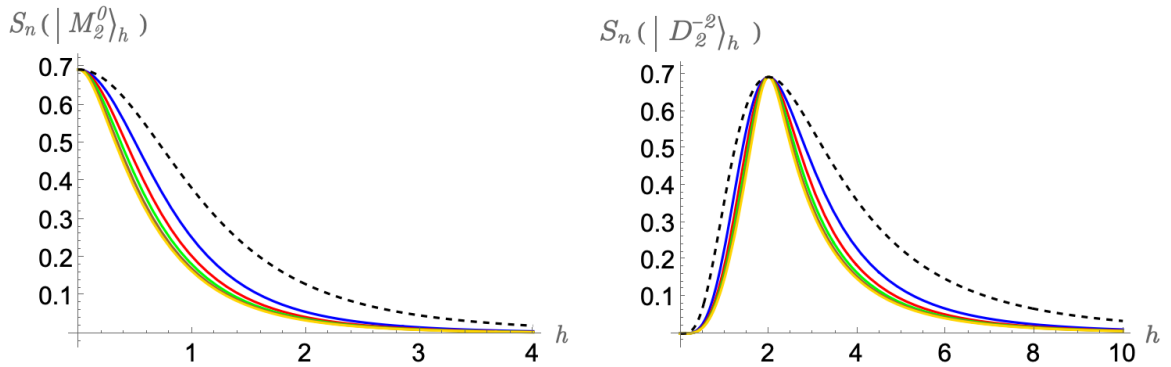


Figure 6: Rényi entropies for the deformed states of two qubits $|M_2^0\rangle_h$ (left) and $|D_2^{-2}\rangle_h$ (right) as a function of the deformation parameter for $n = 2$ (blue), $n = 3$ (red), $n = 4$ (green), $n = 5$ (brown) and $n = 6$ (yellow). The dashed black line corresponds to the von Neumann entropy.

Figure 7 shows the Rényi entropies as a function of the Rényi index n for various two-qubit states, both undeformed, q -deformed and h -deformed, in order to compare the degree of entanglement among these states as n varies. The Rényi entropy of $|M_2^0\rangle_q$ is simply given by

$$S_n(|M_2^0\rangle_q) = \frac{1}{1-n} \log \left[\left(\left(\frac{1}{q+1} \right)^n + \left(\frac{q}{q+1} \right)^n \right) \right]. \quad (55)$$

We can see that all curves decrease as n increases, which is a typical property of Rényi entropies. This reflects the fact that higher n values give more weight to the largest eigenvalues of the reduced density matrix, thus reducing the entropy. The original Bell state (undeformed one) has maximum entanglement, as seen by the constant entropy $\log(2)$ for all values of n . Deformations with parameters q and h reduce the entanglement, with h -deformation being more destructive. As the Rényi index increases, the Rényi entropy for deformed states drops more sharply, indicating the reduced density matrix spectrum becomes more uneven (a signature of lower entanglement). This demonstrates that deformation can be used as a tool to control or tune the entanglement degree in a two-qubit quantum system.

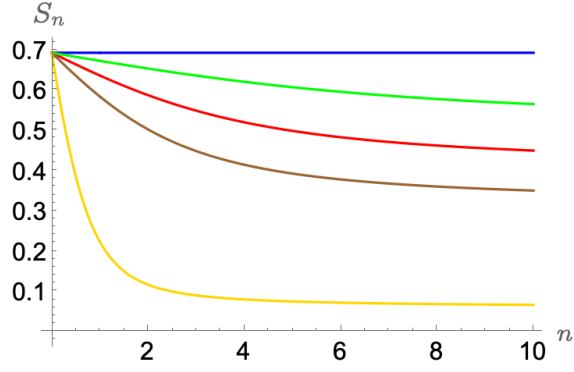


Figure 7: Rényi entropies for the undeformed state of two qubits $(|\uparrow\downarrow\rangle - |\downarrow\uparrow\rangle)/\sqrt{2}$ (blue) and for the deformed ones: $|M_2^0\rangle_{q=0.5}$ (red), $|M_2^0\rangle_{q=1.5}$ (green), $|M_2^0\rangle_{h=0.5}$ (brown) and $|M_2^0\rangle_{h=1.5}$ (yellow) as a function of the index n .

The fidelities between the h -deformed states and their corresponding undeformed ones for two qubits are shown in Fig. 8 and can be written as:

$$F(|D_2^{-2}\rangle_{h=0}, |D_2^{-2}\rangle_h) = \frac{16}{(h^2 + 4)^2}, \quad F(|M_2^0\rangle_{h=0}, |M_2^0\rangle_h) = \frac{2}{2 + h^2}. \quad (56)$$

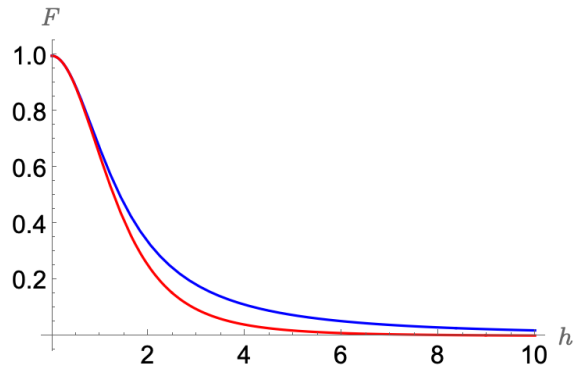


Figure 8: Fidelity between the h -deformed states $|M_2^0\rangle_h$ (blue) and $|D_2^{-2}\rangle_h$ (red) and their corresponding undeformed states as a function of the deformation parameter.

For both $|M_2^0\rangle_h$ (blue) and $|D_2^{-2}\rangle_h$ (red), F starts at 1 when $h = 0$, since the states coincide exactly in the absence of deformation. As h increases, the fidelity drops steadily toward zero. This indicates that larger deformations push each deformed state farther away from its undeformed counterpart. $|D_2^{-2}\rangle_h$ is more sensitive to the deformation h than $|M_2^0\rangle_h$. By the time $h \approx 6$ or larger, both fidelities have dropped below 0.1. This means the deformed states are nearly orthogonal to their original (undeformed) versions. In algebraic or physically motivated deformations, the deformation parameter “bends” or “distorts” the structure of the Hilbert space, that can be described by a deformed inner product in the Hilbert space [59]. As the deformation parameter grows the overlap (inner product) between each deformed state and its undeformed ancestor shrinks rapidly. The fact that $|D_2^{-2}\rangle_h$ loses fidelity faster than $|M_2^0\rangle_h$ suggests that the former’s algebraic or tensor-product structure is more drastically reshaped by the h -deformation. In quantum information terms, a fidelity near zero for large h means that one could effectively distinguish (or even orthogonalize) the deformed state from the original one with near certainty.

Concerning systems of 3 qubits, different kind of entanglement measures has been discussed in [31]. Any system consisting of three subsystems can be split into two parts in three different ways (see Fig. 9). In this section we will see how is the entanglement between a single party A and the composite system BC , written $A|BC$, related to the pairwise entanglement $A|B$ and $A|C$.

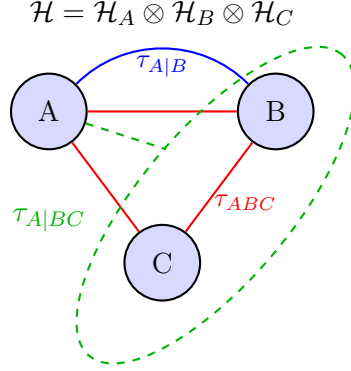


Figure 9: Different tangles in a tripartite system.

In particular, the average tangle of a pure state with respect to all possible 1 + 2 splittings reads

$$\tau_1(|\psi_{ABC}\rangle) = \frac{1}{3} (\tau_{A|BC} + \tau_{B|AC} + \tau_{C|AB}), \quad (57)$$

where

$$\tau_{A|BC} = 4 |\det \text{Tr}_B \text{Tr}_C \rho_{ABC}|, \quad (58)$$

being $\rho_{ABC} = |\psi_{ABC}\rangle \langle \psi_{ABC}|$. The monogamy relation $\tau_{A|BC} \geq \tau_{A|B} + \tau_{A|C}$ must be fulfilled.

We collect here the result of this measure of entanglement only for the h -deformed states (see also Fig. 10):

$$\begin{aligned} \tau_1(|D_3^{-3}\rangle_h) &= \frac{24h^4 (11h^4 + 64h^2 + 48)}{(19h^4 + 32h^2 + 16)^2}, & \tau_1(|D_3^{-1}\rangle_h) &= \frac{128 (67h^4 + 64h^2 + 48)}{3 (9h^4 + 32h^2 + 48)^2}, \\ \tau_1(|M_3^{-1}\rangle_h) &= \frac{8 (4 (h^2 + 4) h^2 + 9)}{3 (5h^2 + 6)^2}, & \tau_1(|M_3^1\rangle_h) &= \frac{24}{(9h^2 + 6)^2}, \\ \tau_1(|V_3^{-1}\rangle_h) &= \tau_1(|V_3^1\rangle_h) = \frac{8}{3 (h^2 + 2)^2}. \end{aligned} \quad (59)$$

The 2 + 1 tangle represents the average entanglement contained in all possible two-partite reductions:

$$\tau_2(|\psi_{ABC}\rangle) = \frac{1}{3} (\tau_{A|B} + \tau_{B|C} + \tau_{C|A}), \quad (60)$$

where [60]

$$\tau_{A|B} = \max (\delta_1 - \delta_2 - \delta_3 - \delta_4, 0), \quad (61)$$

being δ_i the square roots of the eigenvalues (in decreasing order for obtaining a positive quantity) of $(\text{Tr}_C \rho_{ABC}) (\sigma_y^A \otimes \sigma_y^B) (\text{Tr}_C \rho_{ABC})^* (\sigma_y^A \otimes \sigma_y^B)$, where $*$ means complex conjugate and σ_y is the Pauli matrix applied to the corresponding part of the system. By construction, the quantities τ_1, τ_2 are non-negative. We show here the result of this measure of entanglement for the previous discussed states (see also Fig. 10):

$$\begin{aligned} \tau_2(|D_3^{-3}\rangle_h) &= \frac{12h^4 (11h^4 - 8h^2 + 48)}{(19h^4 + 32h^2 + 16)^2}, & \tau_2(|D_3^{-1}\rangle_h) &= \frac{64 (67h^4 - 104h^2 + 48)}{3 (9h^4 + 32h^2 + 48)^2}, \\ \tau_2(|M_3^{-1}\rangle_h) &= \frac{4 (4h^4 - 8h^2 + 9)}{3 (5h^2 + 6)^2}, & \tau_2(|M_3^1\rangle_h) &= \frac{4}{3 (3h^2 + 2)^2}, \\ \tau_2(|V_3^{-1}\rangle_h) &= \tau_2(|V_3^1\rangle_h) = \frac{4}{3 (h^2 + 2)^2}. \end{aligned} \quad (62)$$

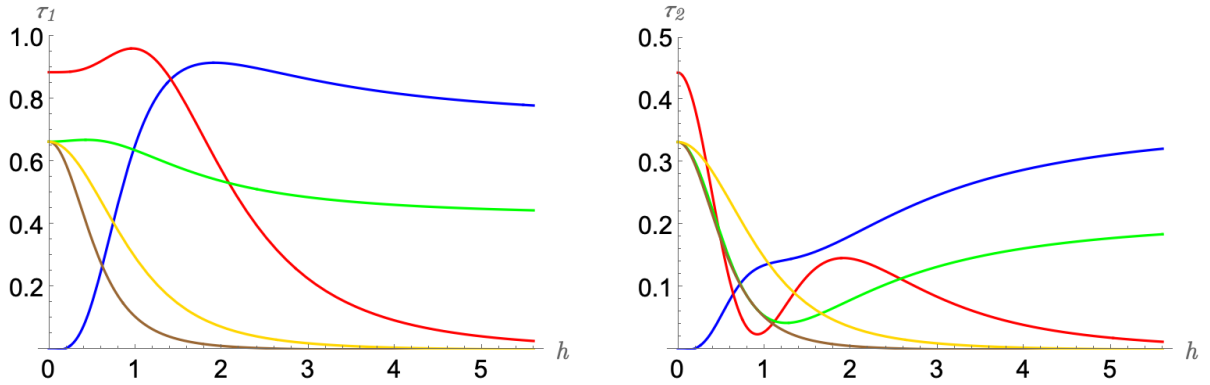


Figure 10: τ_1 (left) and τ_2 (right) for the h -deformed states $|D_3^{-3}\rangle_h$ (blue), $|D_3^{-1}\rangle_h$ (red), $|M_3^{-1}\rangle_h$ (green), $|M_3^1\rangle_h$ (brown) and $|V_3^{-1}\rangle_h$ (yellow) as a function of the deformation parameter.

We can see that for all states except from $|D_3^{-3}\rangle_h$, τ_1 starts at a finite value for $h = 0$ and decreases as h increases, indicating that the global entanglement is sensitive to deformation. $|D_3^{-3}\rangle_h$ grows until $|h| = 1.916$ and then saturates, while $|D_3^{-1}\rangle_h$ shows a peak for $|h| = 0.965$ and then goes to zero. $|M_3^{-1}\rangle_h$ is the state which shows less sensitivity to h compared to the others. Only $|D_3^{-3}\rangle_h$ and $|M_3^{-1}\rangle_h$ exhibits saturation behaviors as h grows, which corresponds to $\tau_1 = 0.731$ and 0.427 , respectively. For all other h -deformed states the entanglement goes to zero for large deformations.

The τ_2 values are generally lower than τ_1 , reflecting the monogamy of entanglement: the more entanglement is shared globally, the less can be shared pairwise. These results highlight the tunability of entanglement structure in h -deformed states, which is relevant for quantum information protocols where specific types of multipartite entanglement are desired (sometimes you want strong pairwise entanglement, sometimes strong global entanglement). We can observe that, as for τ_1 , the states $|D_3^{-3}\rangle_h$, $|D_3^{-1}\rangle_h$, and $|M_3^{-1}\rangle_h$ exhibit a different behavior in comparison with the others, which goes to zero for increasing values of h . For $|D_3^{-1}\rangle_h$, there is a global maximum in $h = 0$, a local minimum in $|h| = 0.919$, a local maximum in $|h| = 1.911$, and finally the function goes to zero. For $|D_3^{-3}\rangle_h$, there is an increasing value of τ_2 as h increases, saturating to $\tau_2 = 0.366$. Finally, for $|M_3^{-1}\rangle_h$ there is a maximum in $h = 0$, a global minimum in $|h| = 1.252$ and then the function saturates to $\tau_2 = 0.213$.

Finally, the average tangle of a pure state of all the system, which characterises the global entanglement, is

$$\tau_3(|\psi_{ABC}\rangle) = \tau_{A|BC} - \tau_{A|B} - \tau_{A|C}. \quad (63)$$

For our deformed states of 3 qubits, it translates into:

$$\begin{aligned} \tau_3(|D_3^{-3}\rangle_h) &= 1728 \frac{h^6}{(19h^4 + 32h^2 + 16)^2}, & \tau_3(|D_3^{-1}\rangle_h) &= 7168 \frac{h^2}{(9h^4 + 32h^2 + 48)^2}, \\ \tau_3(|M_3^{-1}\rangle_h) &= 64 \frac{h^2}{(5h^2 + 6)^2}, & \tau_3(|M_3^1\rangle_h) &= \tau_3(|V_3^{-1}\rangle_h) = \tau_3(|V_3^1\rangle_h) = 0, \end{aligned} \quad (64)$$

which is represented in Fig. 11 (left) as a function of the deformation parameter. This quantity τ_3 , invariant with respect to permutation of the parties, is also called residual entanglement, as it marks the fraction of entanglement which cannot be described by any two-body measures. Note that all of the above formulas for τ_1, τ_2, τ_3 are even functions in h . In Fig. 11 (left) we can see that only the states $|D_3^{-3}\rangle_h, |D_3^{-1}\rangle_h, |M_3^{-1}\rangle_h$, with maxima of values for $|h| = 1.625, 0.931, 1.095$ respectively, have non-zero residual entanglement. The other states have no residual entanglement, meaning that any entanglement present is limited to bipartite correlations. As h increases, tripartite entanglement tends to disappear, as also happens for bipartite and global entanglement for $|D_3^{-1}\rangle_h$ (but not for $|D_3^{-3}\rangle_h$ and $|M_3^{-1}\rangle_h$).

Regarding the fidelity, when comparing the h -deformed states of 3 qubits with their corresponding deformed counterparts, we find

$$\begin{aligned}
F(|D_3^{-3}\rangle_{h=0}, |D_3^{-3}\rangle_h) &= \frac{16}{19h^4 + 32h^2 + 16}, & F(|D_3^{-1}\rangle_{h=0}, |D_3^{-1}\rangle_h) &= \frac{48}{9h^4 + 32h^2 + 48}, \\
F(|M_3^{-1}\rangle_{h=0}, |M_3^{-1}\rangle_h) &= \frac{6}{5h^2 + 6}, & F(|M_3^1\rangle_{h=0}, |M_3^1\rangle_h) &= \frac{2}{3h^2 + 2}, \\
F(|V_3^{-1}\rangle_{h=0}, |V_3^{-1}\rangle_h) &= F(|V_3^1\rangle_{h=0}, |V_3^1\rangle_h) &= \frac{2}{h^2 + 2}. & (65)
\end{aligned}$$

The results are plotted in Fig. 11 (right). Fidelity decreases with h for all states, which means that they move further and further away from the undeformed state $h = 0$. The rate at which fidelity decreases depends on the state: $|D_3^{-3}\rangle_h$ and $|D_3^{-1}\rangle_h$ lose fidelity more rapidly for increasing h compared to $|V_3^{-1}\rangle_h$ and $|M_3^{-1}\rangle_h$. $|M_3^1\rangle_h$ shows intermediate behavior.

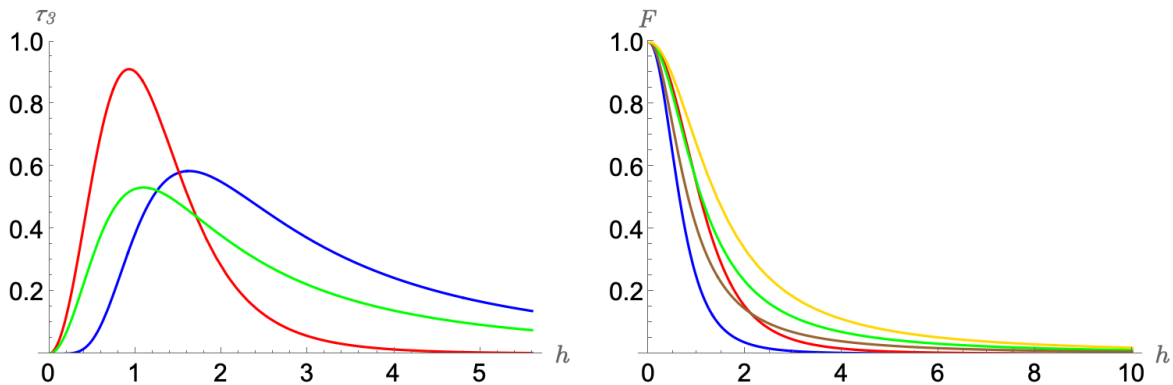


Figure 11: τ_3 (left) and fidelity (right) for the h -deformed states $|D_3^{-3}\rangle_h$ (blue), $|D_3^{-1}\rangle_h$ (red), $|M_3^{-1}\rangle_h$ (green), $|M_3^1\rangle_h$ (brown) and $|V_3^{-1}\rangle_h$ (yellow) as a function of the deformation parameter.

7 Conclusions

In this work, we have explored the application of the Jordanian quantum algebra $\mathcal{U}_h(sl(2, \mathbb{R}))$ to the study of entanglement properties in quantum states. We have developed a systematic approach to construct h -deformed Dicke states for multi-qubit systems, providing explicit formulations for up to four qubits and a general method for larger systems. We have analyzed various measures of entanglement, including von Neumann entropy, Rényi entropy, and fidelity, for h -deformed states. We have compared h -deformed states with their q -deformed counterparts, highlighting similarities and differences in their entanglement properties. This comparison provides insights into the unique features of h -deformation. Our results show that the deformation parameter h can be used to control the degree of entanglement in these states.

Our analysis of density matrices for h -deformed states suggests that these states might be useful in describing noise and decoherence effects in experimental settings. Moreover, the h -deformation provides a new tool for manipulating and studying entangled states, which could have applications in quantum computing, quantum communication, and other areas of quantum information science.

Future work could focus on extending this analysis to larger multi-qubit systems, exploring potential applications in quantum error correction, and investigating experimental implementations of h -deformed states. Additionally, further comparative studies with the standard deformation could provide a more comprehensive understanding of the role of deformations in quantum entanglement.

Acknowledgments

The authors acknowledge partial support from the grant PID2023-148373NB-I00 funded by MCIN/AEI/10.13039/501100011033/FEDER – UE, and the Q-CAYLE Project funded by the Regional Gov-

ernment of Castilla y León (Junta de Castilla y León) and the Ministry of Science and Innovation MICIN through NextGenerationEU (PRTR C17.I1).

References

- [1] E. Abe. *Hopf Algebras*. Cambridge Tracts in Mathematics. Cambridge University Press, Cambridge, 2004.
- [2] V Chari and A. N. Pressley. *A guide to quantum groups*. Cambridge University Press, 1994.
- [3] S. Majid. *Foundations of Quantum Group Theory*. Cambridge University Press, Cambridge, 1995.
- [4] V. G. Drinfel'd. Quantum Groups. In A. Gleason, editor, *Proc. Int. Congr. Math. (Berkeley 1986)*, pages 798–820, Providence RI, 1987. American Mathematical Society.
- [5] M Jimbo. A q -difference analogue of $U(g)$ and the Yang-Baxter equation. *Letters in Mathematical Physics*, 10(1):63–69, 1985.
- [6] S. Majid. Hopf Algebras for Physics at the Planck Scale. *Class. Quant. Grav.*, 5:1587–1606, 1988.
- [7] C Gómez, M Ruiz-Altaba, and G Sierra. *Quantum Groups in Two-Dimensional Physics*. Cambridge University Press, 1996.
- [8] M. Chaichian and A. Demichev. *Introduction to Quantum Groups*. World Scientific Publishing, 1996.
- [9] D. Bonatsos and C. Daskaloyannis. Quantum groups and their applications in nuclear physics. *Prog. Part. Nucl. Phys.*, 43:537–618, 1999.
- [10] R J. Szabo. Quantum field theory on noncommutative spaces. *Phys. Rept.*, 378:207–299, 2003.
- [11] A. Addazi et al. Quantum gravity phenomenology at the dawn of the multi-messenger era—A review. *Prog. Part. Nucl. Phys.*, 125:103948, 2022.
- [12] P. P. Kulish and N. Yu. Reshetikhin. Quantum linear problem for the Sine-Gordon equation and higher representation. *Zap. Nauchn. Semin.*, 101:101–110, 1981.
- [13] V. Pasquier and H. Saleur. Common structures between finite systems and conformal field theories through quantum groups. *Nuclear Physics B*, 330:523–556, 1990.
- [14] E. E. Demidov, Yu. I. Manin, E. E. Mukhin, and D. V. Zhdanovich. Non-Standard Quantum Deformations of $GL(n)$ and Constant Solutions of the Yang-Baxter Equation. *Progress of Theoretical Physics Supplement*, 102:203–218, 1990.
- [15] S. Zakrzewski. A Hopf star-algebra of polynomials on the quantum $SL(2, \mathbb{R})$ for a ‘unitary’ R-matrix. *Letters in Mathematical Physics*, 22(4):287–289, 1991.
- [16] Ch Ohn. A*-product on $SL(2)$ and the corresponding nonstandard $sl(2)$. *Letters in mathematical physics*, 25(2):85–88, 1992.
- [17] A. Ballesteros and F. J. Herranz. Universal R-matrix for non-standard quantum $sl(2, \mathbb{R})$. *J. Phys. A: Math. Gen.*, 29(13):L311, 1996.
- [18] V. K. Dobrev. Representations of the Jordanian quantum algebra $U_h(sl(2))$. *IC-96-14, Trieste*, 1996.

- [19] B. Abdesselam, A. Chakrabarti, and R. Chakrabarti. Irreducible representations of Jordanian Quantum algebra $\mathcal{U}_h(sl(2))$ via a nonlinear map. *Modern Physics Letters A*, 11(36):2883–2891, 1996.
- [20] A. Ballesteros, F J. Herranz, and J. Negro. Boson representations, non-standard quantum algebras and contractions. *J. Phys. A: Math. Gen.*, 30:6797, 1997.
- [21] N Aizawa. Irreducible decomposition for tensor product representations of Jordanian quantum algebras. *Journal of Physics A: Mathematical and General*, 30(17):5981, 1997.
- [22] J Van der Jeugt. Representations and Clebsch-Gordan coefficients for the Jordanian quantum algebra. *J. Phys. Math. Gen.*, 31(5):1495, 1998.
- [23] A Ballesteros, R Ramírez, and M Reboiro. Non-standard quantum algebras and finite dimensional \mathcal{PT} -symmetric systems. *J. Phys. A: Math. Theor.*, 57(3):035202, 2024.
- [24] A. Ballesteros, R. Ramírez, and M. Reboiro. Non-standard quantum algebras and infinite-dimensional \mathcal{PT} -symmetric systems. arXiv:2504.21833 , 2025.
- [25] L Amico, R Fazio, A Osterloh, and V Vedral. Entanglement in many-body systems. *Rev. Mod. Phys.*, 80:517–576, 2008.
- [26] J. Eisert, M. Cramer, and M. B. Plenio. Colloquium: Area laws for the entanglement entropy. *Rev. Mod. Phys.*, 82:277–306, 2010.
- [27] P Calabrese, J Cardy, and B Doyon. Entanglement entropy in extended quantum systems. *J. Phys. A: Math. Theor.*, 42(50):500301, 2009.
- [28] O A. Castro-Alvaredo and L. Santamaría-Sanz. Symmetry-resolved measures in quantum field theory: A short review. *Modern Physics Letters B*, 39(07):2430002, 2025.
- [29] W. et al Wieczorek. Experimental Entanglement of a Six-Photon Symmetric Dicke State. *Phys. Rev. Lett.*, 103(2):020504, 2009.
- [30] R. et al Prevedel. Experimental Realization of Dicke States of up to Six Qubits for Multiparty Quantum Networking. *Phys. Rev. Lett.*, 103(2):020503, 2009.
- [31] I. Bengtsson and K. Życzkowski. *Geometry of Quantum States: An Introduction to Quantum Entanglement*. Cambridge University Press, 2006.
- [32] M. Walter, D. Gross, and J. Eisert. Multipartite entanglement. *Quantum Information: From Foundations to Quantum Technology Applications*, pages 293–330, 2016.
- [33] B. L. van der Waerden. *Group Theory and Quantum Mechanics*. Springer-Verlag, 1932.
- [34] H Georgi. *Lie algebras in particle physics*, volume 54. Perseus Books, Reading, MA, 2nd ed. edition, 1999.
- [35] L. C. Biedenharn and M. A. Lohe. *Quantum group symmetry and q tensor algebras*. World Scientific Pub Co Inc, 1996.
- [36] J Sakurai and J Napolitano. *Modern Quantum Mechanics*. Quantum physics, quantum information and quantum computation. Cambridge University Press, 2020.
- [37] R. Álvarez-Nodarse and A. Arenas-Gómez. The q -Analog of the Quantum Theory of Angular Momentum: a Review from Special Functions. *Russian Journal of Mathematical Physics*, 31(1):24–43, 2024.
- [38] ZH Li and AM Wang. Entanglement entropy in quasi-symmetric multi-qubit states. *International Journal of Quantum Information*, 13(02):1550007, 2015.

- [39] N Aizawa. Irreducible decomposition for tensor product representations of Jordanian quantum algebras. *J. Phys. A: Math. Gen.*, 30:5981, 1997.
- [40] J Van der Jeugt. Representations and Clebsch-Gordan coefficients for the Jordanian quantum algebra. *J. Phys. A: Math. Gen.*, 31:1495, 1998.
- [41] A. Ballesteros, I. Gutiérrez-Sagredo, V. Mariscal, and J. J. arXiv: 2502.20884 Relancio. Quantum group deformation of the Kittel–Shore model. 2025.
- [42] H. J. Kimble. The quantum internet. *Nature*, 453(7198):1023–1030, 2008.
- [43] JF Poyatos, R Walser, JI Cirac, P Zoller, and R Blatt. Motion tomography of a single trapped ion. *Phys. Rev. A*, 53(4):R1966, 1996.
- [44] H G. et al Stemp. Tomography of entangling two-qubit logic operations in exchange-coupled donor electron spin qubits. *Nature Communications*, 15(1):8415, 2024.
- [45] N et al Kiesel. Experimental observation of four-photon entangled Dicke state with high fidelity. *Phys. Rev. Lett.*, 98(6):063604, 2007.
- [46] R et al Krischek. Ultraviolet enhancement cavity for ultrafast nonlinear optics and high-rate multiphoton entanglement experiments. *Nature Photonics*, 4(3):170–173, 2010.
- [47] R. et al Stricker. Experimental deterministic correction of qubit loss. *Nature*, 585(7824):207–210, 2020.
- [48] R. et al Stricker. Characterizing quantum instruments: From nondemolition measurements to quantum error correction. *PRX Quantum*, 3(3):030318, 2022.
- [49] C. et al Schwemmer. Experimental comparison of efficient tomography schemes for a six-qubit state. *Phys. Rev. Lett.*, 113(4):040503, 2014.
- [50] D Binosi, G Garberoglio, D Maragnano, M Dapor, and M Liscidini. A tailor-made quantum state tomography approach. *APL Quantum*, 1(3), 2024.
- [51] D. et al Cruz. Efficient quantum algorithms for GHZ and W states, and implementation on the IBM quantum computer. *Advanced Quantum Technologies*, 2(5-6):1900015, 2019.
- [52] S Aktar, A Bärtschi, A A Badawy, and S Eidenbenz. A divide-and-conquer approach to Dicke state preparation. *IEEE Transactions on Quantum Engineering*, 3:1–16, 2022.
- [53] E Schmidt. Zur Theorie der linearen und nichtlinearen Integralgleichungen. *Mathematische Annalen*, 63(4):433–476, 1907.
- [54] A. K. Ekert and P. L. Knight. Entangled Quantum Systems and the Schmidt Decomposition. *American Journal of Physics*, 63(5):415–423, 1995.
- [55] A. Acín, A. Andrianov, L. Costa, E. Jane, J. I. Latorre, and R. Tarrach. Generalized Schmidt Decomposition and Classification of Three-Quantum-Bit States. *Phys. Rev. Lett.*, 85:1560–1563, 2000.
- [56] U. Schollwöck. The density-matrix renormalization group in the age of matrix product states. *Annals of Physics*, 326:96–192, 2011.
- [57] M. A. Nielsen. Conditions for a Class of Entanglement Transformations. *Phys. Rev. Lett.*, 83:436–439, 1999.
- [58] G. Benenti, G. Casati, D. Rossini, and G. Strini. *Principles of Quantum Computation and Information*. World Scientific, 2018.

- [59] A Ballesteros, I Gutierrez-Sagredo, J de Ramon, and J. J. Relancio. Deformations of the symmetric subspace of qubit chains. *arXiv:2503.23554*, 2025.
- [60] V. Kendon, K. Nemoto, and W. Munro. Typical entanglement in multiple-qubit systems. *Journal of Modern Optics*, 49:1709–1716, 2002.

A Acin decomposition for 3-qubit h -deformed states

	$ M_3^1\rangle_h$	$ M_3^{-1}\rangle_h$	$ V_3^1\rangle_h$	$ V_3^{-1}\rangle_h$
U_1	$\begin{pmatrix} \frac{\sqrt{2}}{d} & -\frac{h+\sqrt{4+h^2}}{\sqrt{2d}} \\ h-\sqrt{4+h^2} & \frac{\sqrt{2}}{d} \end{pmatrix}$	$\begin{pmatrix} \frac{\sqrt{2}}{d} & -\frac{h+\sqrt{4+h^2}}{\sqrt{2d}} \\ h-\sqrt{4+h^2} & \frac{\sqrt{2}}{d} \end{pmatrix}$	$\begin{pmatrix} 0 & 1 \\ 1 & 0 \end{pmatrix}$	$\begin{pmatrix} \frac{1}{\sqrt{4h^2+1}} & \frac{2h}{\sqrt{4h^2+1}} \\ -\frac{2h}{\sqrt{4h^2+1}} & \frac{1}{\sqrt{4h^2+1}} \end{pmatrix}$
U_2	$\begin{pmatrix} -\frac{h+\sqrt{4+h^2}}{\sqrt{2d}} & \frac{\sqrt{2}}{d} \\ -\frac{\sqrt{2}}{d} & -\frac{h+\sqrt{4+h^2}}{\sqrt{2d}} \end{pmatrix}$	$\begin{pmatrix} -\frac{h+\sqrt{4+h^2}}{\sqrt{2d}} & \frac{\sqrt{2}}{d} \\ -\frac{\sqrt{2}}{d} & -\frac{h+\sqrt{4+h^2}}{\sqrt{2d}} \end{pmatrix}$	$\begin{pmatrix} 1 & 0 \\ 0 & 1 \end{pmatrix}$	$\begin{pmatrix} \frac{h}{\sqrt{h^2+1}} & \frac{1}{\sqrt{h^2+1}} \\ -\frac{1}{\sqrt{h^2+1}} & \frac{h}{\sqrt{h^2+1}} \end{pmatrix}$
U_3	$\begin{pmatrix} 1 & 0 \\ 0 & 1 \end{pmatrix}$	$\begin{pmatrix} 0 & 1 \\ 1 & 0 \end{pmatrix}$	$\begin{pmatrix} 1 & 0 \\ 0 & 1 \end{pmatrix}$	$\begin{pmatrix} \frac{4h}{\sqrt{16h^2+1}} & -\frac{1}{\sqrt{16h^2+1}} \\ \frac{1}{\sqrt{16h^2+1}} & \frac{4h}{\sqrt{16h^2+1}} \end{pmatrix}$
λ_0	$\frac{\sqrt{2}}{h^2-h\sqrt{h^2+4}+2}$	$\frac{\sqrt{2}}{h^2-h\sqrt{h^2+4}+2}$	$-\frac{1}{\sqrt{6}}$	$-\frac{16h^4+17h^2+1}{\sqrt{6}\sqrt{h^2+1}\sqrt{4h^2+1}\sqrt{16h^2+1}}$
λ_1	0	0	$-\sqrt{\frac{3}{2}}h$	$-\frac{h(10h^2+7)}{\sqrt{6}\sqrt{h^2+1}\sqrt{4h^2+1}\sqrt{16h^2+1}}$
λ_2	0	0	$\sqrt{\frac{2}{3}}$	$\sqrt{\frac{2}{3}}\frac{4h^4-3h^2-1}{\sqrt{h^2+1}\sqrt{4h^2+1}\sqrt{16h^2+1}}$
λ_3	$\frac{1}{\sqrt{2}}$	$\frac{1}{\sqrt{2}}$	$-\sqrt{\frac{1}{6}}$	$\frac{\sqrt{4h^2+1}}{\sqrt{6}\sqrt{h^2+1}\sqrt{16h^2+1}}$
λ_4	0	0	0	$-2\sqrt{\frac{2}{3}}\frac{h\sqrt{4h^2+1}}{\sqrt{h^2+1}\sqrt{16h^2+1}}$

Table 1: Acin decomposition of the states of 3 qubits $\{|M_3^{-1}\rangle_h, |M_3^1\rangle_h, |V_3^{-1}\rangle_h, |V_3^1\rangle_h\}$ (where $j = 1/2$). In this table the matrices U_1, U_2, U_3 such that $|\tilde{\Psi}\rangle_h = U_1 \otimes U_2 \otimes U_3 |\Psi\rangle_h$ are collected as well as the coefficients $\lambda_0, \lambda_1, \lambda_2, \lambda_3$ of eq. (45). $|\tilde{\Psi}\rangle_h$ corresponds to the Acin decomposition of the state $|\Psi\rangle_h$. Notice that coefficients a, b, c, d are given in Eqs. (37) and (42).

	$ D_3^{-3}\rangle_h$	$ D_3^{-1}\rangle_h$
U_1	$\begin{pmatrix} \frac{2}{\sqrt{(4\sqrt{3}+7)h^2+4}} & \frac{(\sqrt{3}+2)h}{\sqrt{(4\sqrt{3}+7)h^2+4}} \\ -\frac{(\sqrt{3}+2)h}{\sqrt{(4\sqrt{3}+7)h^2+4}} & \frac{2}{\sqrt{(4\sqrt{3}+7)h^2+4}} \end{pmatrix}$	$\begin{pmatrix} \frac{2}{\sqrt{(4\sqrt{7}+11)h^2+4}} & \frac{(\sqrt{7}+2)h}{\sqrt{(4\sqrt{7}+11)h^2+4}} \\ -\frac{(\sqrt{7}+2)h}{\sqrt{(4\sqrt{7}+11)h^2+4}} & \frac{2}{\sqrt{(4\sqrt{7}+11)h^2+4}} \end{pmatrix}$
U_2	$\begin{pmatrix} \frac{h}{\sqrt{h^2+\frac{4}{3}}} & \frac{2}{\sqrt{3h^2+4}} \\ -\frac{2}{\sqrt{3h^2+4}} & \frac{h}{\sqrt{h^2+\frac{4}{3}}} \end{pmatrix}$	$\begin{pmatrix} \frac{h}{\sqrt{h^2+\frac{4}{7}}} & \frac{2}{\sqrt{7h^2+4}} \\ -\frac{2}{\sqrt{7h^2+4}} & \frac{h}{\sqrt{h^2+\frac{4}{7}}} \end{pmatrix}$
U_3	$\begin{pmatrix} \frac{h}{\sqrt{h^2-16\sqrt{3}+28}} & \frac{2}{(\sqrt{3}+2)\sqrt{h^2-16\sqrt{3}+28}} \\ -\frac{2}{(\sqrt{3}+2)\sqrt{h^2-16\sqrt{3}+28}} & \frac{h}{\sqrt{h^2-16\sqrt{3}+28}} \end{pmatrix}$	$\begin{pmatrix} \frac{h}{\sqrt{h^2+\frac{4}{4\sqrt{7}+11}}} & \frac{2}{(\sqrt{7}+2)\sqrt{h^2+\frac{4}{4\sqrt{7}+11}}} \\ -\frac{2}{(\sqrt{7}+2)\sqrt{h^2+\frac{4}{4\sqrt{7}+11}}} & \frac{h}{\sqrt{h^2+\frac{4}{4\sqrt{7}+11}}} \end{pmatrix}$
λ_0	$\frac{h\sqrt{4\sqrt{3}+7}\sqrt{3h^2+4}((7\sqrt{3}+12)h^2+4\sqrt{3})}{4(\sqrt{3}+2)((4\sqrt{3}+7)h^2+4)}$	$\frac{\sqrt{12\sqrt{7}+33}\sqrt{7h^2+4}}{6(\sqrt{7}+2)}$
λ_1	$\frac{\sqrt{4\sqrt{3}+7}(h^2+4)}{2(\sqrt{3}+2)\sqrt{3h^2+4}}$	$\frac{\sqrt{7(4\sqrt{7}+11)h(4-3h^2)}}{4(\sqrt{7}+2)\sqrt{3(7h^2+4)}}$
λ_2	$-\frac{h\sqrt{4\sqrt{3}+7}(3h^2-4)((7\sqrt{3}+12)h^2+4\sqrt{3})}{4(\sqrt{3}+2)\sqrt{3h^2+4}((4\sqrt{3}+7)h^2+4)}$	$\frac{\sqrt{12\sqrt{7}+33}(7h^2-4)}{6(\sqrt{7}+2)\sqrt{7h^2+4}}$
λ_3	$\frac{\sqrt{3(4\sqrt{3}+7)h(h^2+4)}}{4(\sqrt{3}+2)\sqrt{3h^2+4}}$	$\frac{\sqrt{(4\sqrt{7}+11)(3h^2-4)}}{2(\sqrt{7}+2)\sqrt{3(7h^2+4)}}$
λ_4	$\frac{3\sqrt{4\sqrt{3}+7}h^2}{(\sqrt{3}+2)\sqrt{3h^2+4}}$	$-\frac{2\sqrt{12\sqrt{7}+33}h((11\sqrt{7}+28)h^2+4\sqrt{7})}{-3(\sqrt{7}+2)\sqrt{7h^2+4}((4\sqrt{7}+11)h^2+4)}$

Table 2: Acin decomposition of the states of 3 qubits $\{|D_3^{-3}\rangle_h, |D_3^{-1}\rangle_h\}$ (characterised by $j = 3/2$). In this table the matrices U_1, U_2, U_3 such that $|\tilde{\Psi}\rangle_h = U_1 \otimes U_2 \otimes U_3 |\Psi\rangle_h$ are collected as well as the coefficients $\lambda_0, \lambda_1, \lambda_2, \lambda_3$ of eq. (45). $|\tilde{\Psi}\rangle_h$ corresponds to the Acin decomposition of the state $|\Psi\rangle_h$. Notice that coefficients a, b, c, d are given in Eqs. (37) and (42).

B Clebsch–Gordan coefficients for 4-qubit h -deformed states

$N = 4$	$ \uparrow\uparrow\uparrow\uparrow\rangle$	$ \uparrow\uparrow\uparrow\downarrow\rangle$	$ \uparrow\uparrow\downarrow\uparrow\rangle$	$ \uparrow\uparrow\downarrow\downarrow\rangle$	$ \uparrow\downarrow\uparrow\uparrow\rangle$	$ \uparrow\downarrow\uparrow\downarrow\rangle$	$ \uparrow\downarrow\downarrow\uparrow\rangle$	$ \uparrow\downarrow\downarrow\downarrow\rangle$	$ \downarrow\uparrow\uparrow\uparrow\rangle$	$ \downarrow\uparrow\uparrow\downarrow\rangle$	$ \downarrow\uparrow\downarrow\uparrow\rangle$	$ \downarrow\uparrow\downarrow\downarrow\rangle$	$ \downarrow\downarrow\uparrow\uparrow\rangle$	$ \downarrow\downarrow\uparrow\downarrow\rangle$	$ \downarrow\downarrow\downarrow\uparrow\rangle$	$ \downarrow\downarrow\downarrow\downarrow\rangle$
D_4^{-4}	1	$-3h/2$	$-h/2$	$h/2$	$3h/2$	$7h^2/4$	$h^2/4$	$-5h^2/4$	$7h^2/4$	$-9h^2/8$	$5h^2/8$	$-5h^2/8$	$-5h^2/8$	$9h^2/8$	$9h^2/8$	$9h^4/16$
D_4^{-2}	0	$1/2$	$1/2$	$-h/2$	$1/2$	$-h$	$h/2$	0	h	$9h^2/8$	$h^2/8$	$h^2/8$	$h^2/8$	$9h^2/8$	0	0
D_4^0	0	0	0	$1/\sqrt{6}$	$1/\sqrt{6}$	$1/\sqrt{6}$	$1/\sqrt{6}$	$1/\sqrt{6}$	$1/\sqrt{6}$	$-h\sqrt{3}/8$	$-h/\sqrt{24}$	$-h/\sqrt{24}$	$h\sqrt{3}/8$	$h\sqrt{3}/8$	$h^2\sqrt{3}/8$	$h^2\sqrt{3}/8$
D_4^2	0	0	0	0	0	0	0	0	0	$1/2$	$1/2$	$1/2$	$1/2$	$1/2$	0	0
D_4^4	0	0	0	0	0	0	0	0	0	0	0	0	0	0	1	1
M_4^{-2}	0	$\sqrt{3}/6$	$\sqrt{3}/6$	$-h\sqrt{3}/6$	$\sqrt{3}/6$	$-h/\sqrt{3}$	$-h\sqrt{3}/6$	$h\sqrt{3}/3$	$-2h\sqrt{3}/3$	$3h^2\sqrt{3}/8$	$-h^2\sqrt{3}/8$	$-h^2\sqrt{3}/8$	$5h^2\sqrt{3}/24$	$-11h^2\sqrt{3}/24$	$-h^3\sqrt{3}/4$	$-h^3\sqrt{3}/4$
M_4^0	0	0	0	$1/\sqrt{6}$	$1/\sqrt{6}$	$1/\sqrt{6}$	$1/\sqrt{6}$	$-1/\sqrt{6}$	$-1/\sqrt{6}$	$-h\sqrt{6}/4$	$-h/(2\sqrt{6})$	$-h/(2\sqrt{6})$	$-h\sqrt{6}/4$	$-5h/(2\sqrt{6})$	0	0
M_4^2	0	0	0	0	0	0	0	0	0	$\sqrt{3}/2$	$-\sqrt{3}/6$	$-\sqrt{3}/6$	$-\sqrt{3}/6$	$-\sqrt{3}/6$	$-h\sqrt{3}$	$-h\sqrt{3}$
V_4^{-2}	0	$1/\sqrt{6}$	$1/\sqrt{6}$	$h\sqrt{6}/12$	$h\sqrt{6}/12$	$-h\sqrt{6}/3$	$h\sqrt{6}/12$	$-h\sqrt{6}/4$	$-h/\sqrt{6}$	$h^2\sqrt{6}/4$	0	0	$-h^2\sqrt{6}/24$	$-5h^2\sqrt{6}/24$	$-h^3\sqrt{6}/8$	$-h^3\sqrt{6}/8$
V_4^0	0	0	0	$\sqrt{3}/6$	$\sqrt{3}/6$	$\sqrt{3}/6$	$\sqrt{3}/6$	$-\sqrt{3}/6$	$-\sqrt{3}/6$	$-h\sqrt{3}/2$	$-h\sqrt{3}/6$	$-h\sqrt{3}/6$	0	$-h\sqrt{3}/3$	0	0
V_4^2	0	0	0	0	0	0	0	0	0	0	$\sqrt{6}/3$	$-\sqrt{6}/3$	$-\sqrt{6}/3$	$-\sqrt{6}/3$	$-h\sqrt{6}/2$	$-h\sqrt{6}/2$
T_4^0	0	0	0	$1/\sqrt{3}$	$1/\sqrt{3}$	$1/\sqrt{3}$	$1/\sqrt{3}$	$1/\sqrt{3}$	$1/\sqrt{3}$	$-h\sqrt{3}/2$	$-h\sqrt{3}/6$	$-h\sqrt{3}/6$	$h\sqrt{3}/6$	$h\sqrt{3}/6$	$h^2\sqrt{3}/2$	$h^2\sqrt{3}/2$
R_4^{-2}	0	$1/\sqrt{2}$	$-1/\sqrt{2}$	$-h/\sqrt{2}$	$h/\sqrt{2}$	$-h/\sqrt{2}$	$-h/\sqrt{2}$	$h/\sqrt{2}$	0	$h^2/\sqrt{8}$	$-h^2/\sqrt{8}$	$-h^2/\sqrt{8}$	$h^2/\sqrt{32}$	$-h^2/\sqrt{32}$	$-h^3/\sqrt{32}$	$-h^3/\sqrt{32}$
R_4^0	0	0	0	$1/2$	$1/2$	$1/2$	$1/2$	$-1/2$	0	$-h/2$	$-h/2$	$-h/2$	0	0	0	0
R_4^2	0	0	0	0	0	0	0	0	0	0	0	0	$1/\sqrt{2}$	$1/\sqrt{2}$	$-1/\sqrt{2}$	$-1/\sqrt{2}$
Q_4^0	0	0	0	$1/2$	$1/2$	$1/2$	$1/2$	$-1/2$	0	$-h/2$	$h/2$	$h/2$	$-h/2$	$h/2$	$h/2$	$h^2/2$

Table 3: Configuration of states of 4 qubits as a linear combination of the elements of the basic/computational basis (in the first row of the table) with the associated Clebsch–Gordan coefficients.